5-2011

Low power design of a 916 MHz Gilbert Cell Mixer and a Class-A Power Amplifier for Bioluminescent Bioreporter Integrated Circuit Transmitter

Supriya Kilambi
UTK, skilambi@utk.edu

To the Graduate Council:

I am submitting herewith a thesis written by Supriya Kilambi entitled "Low power design of a 916 MHz Gilbert Cell Mixer and a Class-A Power Amplifier for Bioluminescent Bioreporter Integrated Circuit Transmitter." I have examined the final electronic copy of this thesis for form and content and recommend that it be accepted in partial fulfillment of the requirements for the degree of Master of Science, with a major in Computer Engineering.

Syed K Islam, Major Professor

We have read this thesis and recommend its acceptance:

Gregory Peterson, Jeremy Holleman

Accepted for the Council:
Carolyn R. Hodges

Vice Provost and Dean of the Graduate School

(Original signatures are on file with official student records.)

To the Graduate Council:

I am submitting herewith a thesis written by Supriya Kilambi entitled "Low Power Design of a 916 MHz Gilbert Cell Mixer and a Class-A Power Amplifier for Bioluminescent Bioreporter Integrated Circuit Transmitter". I have examined the final electronic copy of this thesis for form and content and recommend that it be accepted in partial fulfillment of the requirements for the degree of Master of Science, with a major in Computer Engineering.

Syed K Islam, Major Professor

We have read this thesis
and recommend its acceptance:

Gregory Peterson

Jeremy Holleman

Accepted for the Council:

Carolyn R. Hodges
Vice Provost and Dean of the Graduate School

(Original signatures are on file with official student records.)

Low Power Design of a 916 MHz Gilbert Cell Mixer and a Class-A Power Amplifier for Bioluminescent Bioreporter Integrated Circuit Transmitter

A Thesis

Presented for the

Master of Science

Degree

The University of Tennessee, Knoxville

Supriya Kilambi

May 2011

Dedication

This thesis is dedicated to my parents,

sister and brother-in-law who have

supported me throughout my college career

Acknowledgements

I would like to thank many people who have assisted me while preparing this thesis. I would like to sincerely thank Dr. Syed K. Islam for being my major professor and advisor while attending the University of Tennessee and for his immense support and guidance throughout my Masters program. I would like to thank my thesis committee Dr. Gregory Peterson and Dr. Jeremy Holleman for their time and suggestions. I would like to offer special thanks to Dr. Jeremy Holleman for giving me a lot of advice and explanation about the circuit design and testing.

I am grateful to have the opportunity to finish my Master of Science study in the EECS department of the University of Tennessee. I am thankful to all the professors in the department who taught me valuable knowledge. I am extremely thankful to the MOSIS Educational Program Research (MEP) for supporting the fabrication of the prototype integrated circuit chip. I would like to thank the members of the Analog VLSI laboratory for their help in various aspects. I am thankful to Ashraf B.Islam and Kai Zhu for the valuable suggestions and discussions I had with them. I would like to thank Song for his immense help for testing.

I would like to express my gratitude to EECS department staff especially to Ms. Judy Evans, Ms. Dana Bryson and Mr. Randy Bond for their help with administrative issues. Thanks to everyone in the IT support.

I am thankful to my parents K.V. Pardha Saradhi and Dr. K. Rama Devi for believing in me and supporting me throughout my career. I would like to thank my sister Krishna Priya and my brother-in-law Sharath Bukkapatnam and my nephew Kaustubh Sai Bukkapatnam for their unconditional love.

I am thankful to my cousin Srividya Chilakamarri and my best friends Sai Ajay Kumar Peddu, Divya Raghunathan, Neha Chandra and Harshini Padam for providing sustaining love and inspiration in my joy and solace. I am thankful to Vinay Kumar Mannam, Harshitha Muppaneni, Anuradha Bulusu, Prashanth Kakani, Rama Katakam and all my other friends at UT for the wonderful time I got to spend with them and for the memories that I will cherish forever. I am thankful to my relatives and all my other friends for their support and love during my Masters program.

Abstract

This thesis presents low power design of a 916MHz Gilbert cell mixer and a Class-A power amplifier for the Bioluminescent Bioreporter Integrated Circuit (BBIC) transmitter.

There has been increased use in the man-made sensors that can operate in environments unsuitable for humans and at locations remote from the observer. One such sensor is the bioluminescent bioreporter integrated circuit (BBIC). Bioluminescent bioreporters are the bacteria that are genetically engineered in order to achieve bioluminescence when in contact with a target substance. The BBIC has bioreporters placed on a single CMOS integrated circuit (IC) that detects the bioluminescence, performs the signal processing and finally transmits the senor data. The wireless transmission allows for remote sensing by eliminating the need of costly cabling to communicate with the sensor.

The wireless data transmission is performed by the transmitter system. The digital data stream generated by the signal processing circuitry of the BBIC is ASK modulated for transmission. The direct conversion transmitter used in this design includes a PLL, a mixer and a power amplifier. The PLL is used to generate a 916MHz frequency signal. This signal is mixed with the digital data signal generated from the signal processing circuitry of the BBIC. A double-balanced Gilbert cell is used to perform the mixing operation. The mixer output is applied to a power amplifier that provides amplification of the RF output power. The Gilbert cell mixer and the power amplifier have been implemented in 90nm CMOS process available through MOSIS.

Contents

List of Figures

CHAPTER 1

Introduction

There is an absolute need of human sensing for human interaction in the day-to-day life. We humans probably use and re-use all the five of our senses countless number of times each and every day. However there is a need for the sensing systems which are more accurate, versatile, and selective than a human being could ever be. This resulted in the development of man-made sensors that can make measurements of mechanical, electrical, thermal, and chemical quantities. These man-made sensors can operate in environments unsuitable for humans and at locations remote from the observer.

1.1 Biosensors

A sensor application in which a group of remote sensors are placed throughout an area to be monitored is termed as distributed sensing. One class of sensors that could be helpful in distributed sensing is biosensors. A biosensor combines a biological sensing component with an analytical measuring element to detect, record, and transmit information regarding a physiological change or the presence of various biological materials or chemicals in the environment. In technical terms, a biosensor is a probe that integrates a biological component with an electronic component to yield a measurable signal [Bolton]. Biosensors are used for monitoring changes in the environmental conditions. They come in variety of sizes and shapes and can be used for detection and measurement of concentrations of specific bacteria or hazardous chemicals.

1.2 Whole-Cell Biosensors

The biological component of the biosensor is used to recognize an analyte and subsequently activate a signal that is being detected with a transducer. Immobilized macromolecules such as enzymes or antibodies are used as biological components. Living microorganisms or sections of organs or tissues are also used as biological components. Biosensor in which an intact living cell is used as the biological component is called a whole-cell biosensors. The whole-cell biosensors are considered to be well suited for environmental sensing as they can be made small enough to be used in the field, and are capable of continuous monitoring.

In recent years, there have been increased research and development efforts that have been directed towards the development of new real-time monitoring, *insitu* sensors devices that can be easily deployed in multiple strategic locations for environmental monitoring. These integrated sensors are small and inexpensive and are expected to be monitoring diverse physical environments. There has also been advancement in developing various types of chemical and biological agent sensors, such as bioluminescent bioreporter integrated circuit (BBIC) system developed at the University of Tennessee [Islam].

1.3 Bioluminescent Bioreporter

Bioluminescence is the light produced by a chemical reaction in an organism. For this chemical reaction to occur at least two chemicals are required; a substrate and a luciferase. The oxidation of the substrate is catalyzed by the luciferase. The oxidation results in light and an inactive oxidized product [Bolton]. The reaction is illustrated in Figure 1.1.

Bioreporters essentially contain two genetic elements, a promoter gene and a reporter gene. When the target agent is present in the cell's environment then the promoter gene is turned on (transcribed). In normal bacteria the promoter gene is linked to the other genes that are then likewise turned on and then translated into proteins that help the cell in either adapting or combating to the agent that the cell has been exposed. In case of a bioreporter, these genes are removed and replaced by the reporter genes. As a result, turning on the promoter gene now

causes the reporter gene to be turned on. The promoter/reporter gene complex is transcribed into messenger RNA (mRNA) and then translated into a reporter protein which is responsible for the generation of a detectable signal. Therefore the generation of a signal indicates that the bioreporter has detected a particular target agent in its environment.

Bioluminescent bioreporters are the bacteria that are genetically engineered in order to achieve bioluminescence when in contact with the target substance. These genetically engineered bioreporters can detect and quantify particular chemical agents in soil, air, or water by giving off a measurable bioluminescent signal that is proportional to the concentration of the target substance. The bioluminescent bioreporter gene emits a blue-green light (490-nm) which can be measured rapidly. The amount of light emitted depends upon the level of expression of the reporter gene, and thus upon the exposure level to the inducing pollutant.

1.4 Bioluminescent Bioreporter Integrated Circuit

The technique used to sense bioluminescence in order to detect the presence and concentration of a specific substance is termed as luminometry. The typical measurement of luminescence of a particular bioluminescent bioreporter is done using bench-top luminometers, which use photomultiplier tubes, microchannel plates, or film as detection devices [Bolton]. Although these devices are extremely sensitive they are unfortunately bound to the laboratory because of the cost, size and fragility. Environmental sensing applications that need a large number of distributed measurements are not well served by the present technology. Thus the need for rugged and inexpensive luminometers that can operate in environments outside the laboratory arises.

The concept of the bioluminescent bioreporter integrated circuit (BBIC) is depicted in Figure 1.2 shown below. The bioreporters are placed on a single CMOS integrated circuit (IC) that detects the bioluminescence, executes the signal processing and transmits the senor data. The IC can be assorted into two segments, the microluminometer which includes the integrated photo detection and signal processing, and the transmitter which performs the wireless data transmission. The BBIC is unique in the following two ways – first, it uses a rugged

inexpensive packaging that can be used in many remote applications outside the laboratory for detecting the luminescence of the bioreporters ; second, it combines all the facets of the system into one single small element. The close proximity of the bioreporters to the sensing element wipes out the need for complex instruments to channel the light from the bioreporters to the lumninometer. The wireless transmission allows for remote sensing by eliminating the need of costly cabling to communicate with the sensor. The BBIC is a low power, highly sensitive and inexpensive standalone sensor.

Figure 1.1 Bioluminescence chemical reaction [Bolton]

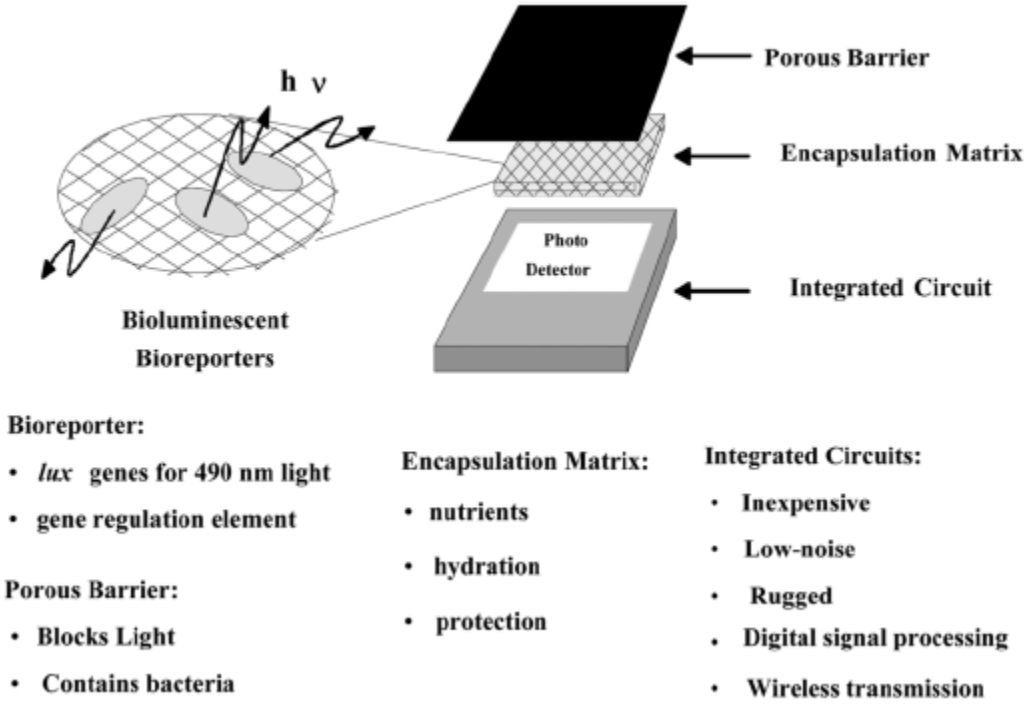

Figure 1.2 Conceptual BBIC system showing the immobilized bioreporters inserted between a porous layer and the integrated circuit with a photodetector [Islam]

1.5 Microluminometer System

The microluminometer is composed of photo detection and signal processing as shown in Figure 1.3. The sensor information, that is, the concentration of the targeted substance is proportional to the intensity of light from the bioreporters. This light is converted by the photodetector into an analog electrical signal. This analog electrical signal is converted into a digital pulse stream by the signal processing circuitry as the light intensity must be eventually processed digitally. Thus the microluminometer performs two signal conversions – optical to analog current, and analog current to digital pulse stream.

1.5.1 Photo Detection

1.5.1.1 Photodiode Operation

A basic p-n junction can be used to convert light into electrical current. When a photon of sufficient energy strikes a semiconductor, the electrons in the valence band absorb the energy of the photons and move to the conduction band if the photon energy exceeds the bandgap energy (E_g). A typical value for E_g in silicon is 1.125 eV. As a result mobile electron and positively charged hole are created. These newly generated carriers contribute to a detectable photocurrent if they cross the p-n junction. The depletion region of the basic p-n junction has a built-in electric field present due to the bound ions resident there. If the carriers are generated in this depletion region then they are swept from the junction by the built-in field of the depletion region. Thus the carriers accelerate towards the contacts of the diode by the electric field. A majority of these carriers contribute to the total generated photocurrent. Carriers generated at a distance greater than a diffusion length from the depletion region have a less probability of becoming a part of the total photocurrent [Bolton]. These electrons generally recombine with holes before they reach the contacts and hence they do not add up to the photocurrent. The effectiveness of the photodetector in converting the light to a detectable electrical current is given by its quantum efficiency.

1.5.1.2 Integrated Photo Detection in CMOS

In a standard CMOS IC process three types of photodiodes are available. These photodiodes are formed by the junctions between p-diffusion/n-well, n-diffusion/p-substrate, and n-well/p-substrate, as shown in Figure 1.4. The p- and n-diffusion regions are highly doped and generally used as the sources/drains of transistors. The p-diffusion/n-well diode is a reasonable choice for detecting the 490nm light generated by the bioreporters as it has a shallow junction depth, but cannot be zero biased resulting in leakage current issues. The n-well/p-substrate diode has a deeper junction depth though it can be zero biased for low leakage. The n-diffusion/p-substrate diode can be zero biased and it also has a shallow junction depth, making it a good choice for integration in the BBIC platform.

A test chip incorporating the three types of photodetectors was fabricated and evaluated in previous work [Bolton]. It was observed from this work that the collection efficiencies for p-diffusion/n-well and n-diffusion/p-substrate diodes were very poor. However, a measured quantum efficiency of 66% at 490nm was observed for the n-well/p-substrate diode. It also provided low leakage current of approximately 70fA for a 1 V reverse bias for a bottom junction area of 8,600 μm^2 [Bolton]. As a result of these tests, the n-well/p-substrate diodes were chosen for use in the BBIC. This detector has an array of small, square n-well electrodes in the p-substrate. This method of arraying small sections decreases the junction area of the total detector which in turn reduces the detector capacitance and leakage currents.

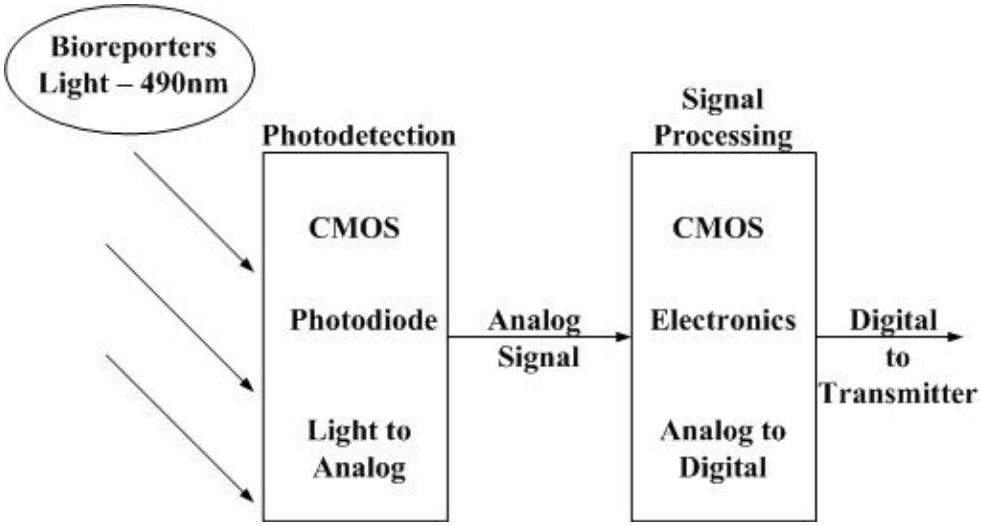

Figure 1.3 Basic microluminometer system operation [Bolton]

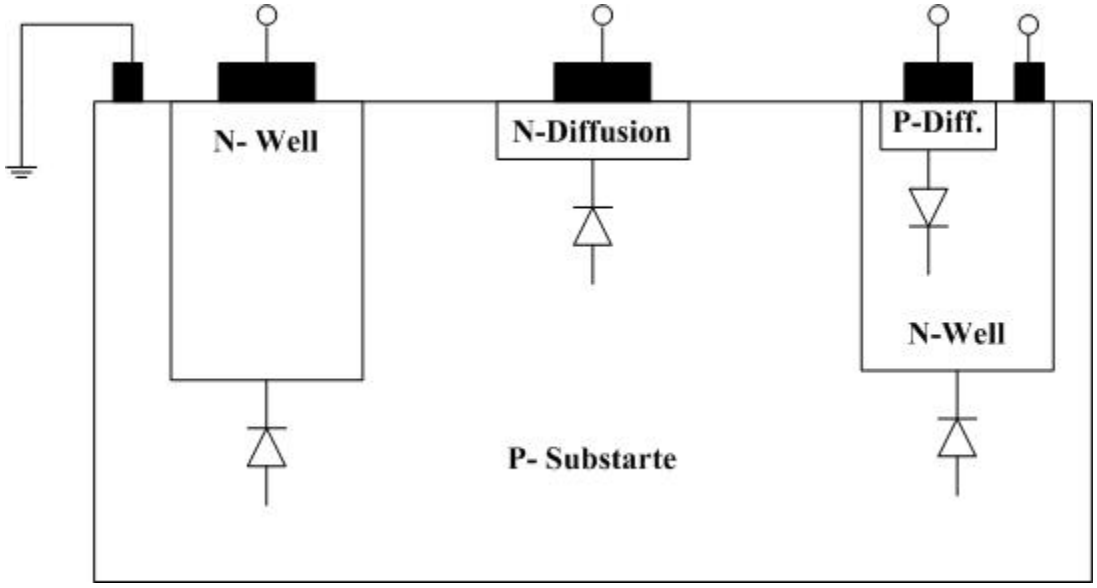

Figure 1.4 Available CMOS photodetectors [Bolton]

1.5.2 Signal Processing Circuitry

The central component of the BBIC is the signal-processing system which is shown in Figure. 1.5. It aims at conversion of the current from the photodiode into a digital signal, the frequency of which is proportional to the concentration of the pollutants. Its operation can be described as follows. During the beginning of the integration process the switches S1 and S2 are closed. This causes the bias on the detector to be set at "ground" and the bias on the output of the integrator to be set at 0.5V. The current from the photodetector is integrated by the integrator for a time T_{int} that is determined by the voltage V_{ref} to the comparator. Whenever the integrator output reaches V_{ref}, the comparator fires. The output of the comparator is used for clocking the one-shot circuitry that produces a pulse of time period T_{reset} that resets the switches S_1 and S_2. The one shot generates a pulse width that guarantees the complete reset of the switches. The output of the one-shot circuitry is used to clock a D flip-flop that is configured as a toggle flip-flop to produce a digital signal whose frequency is given by

$$F_{OUT} = \frac{1}{2(T_{int} + T_{reset})}$$

Whenever a higher concentration of pollutants is sensed by the bioreporter, light of higher intensity is produced thus increasing the photodetector current. The higher current implies a lower integration period decreasing the output frequency. The reverse can be considered for a lower concentration.

It is necessary for the BBIC to be capable of sensing very low concentration of environmental pollutants for which the photodiode and the signal processing circuitry play an important role. The minimum detectable signal (MDS) for the system is a significant specification as it defines the low-end sensitivity of the system. It is inversely proportional to the square root of the total integration time, T_{int}. Thus a measurement system can be considered to be sensitive to low levels of light if it is capable of long integration time [Islam].

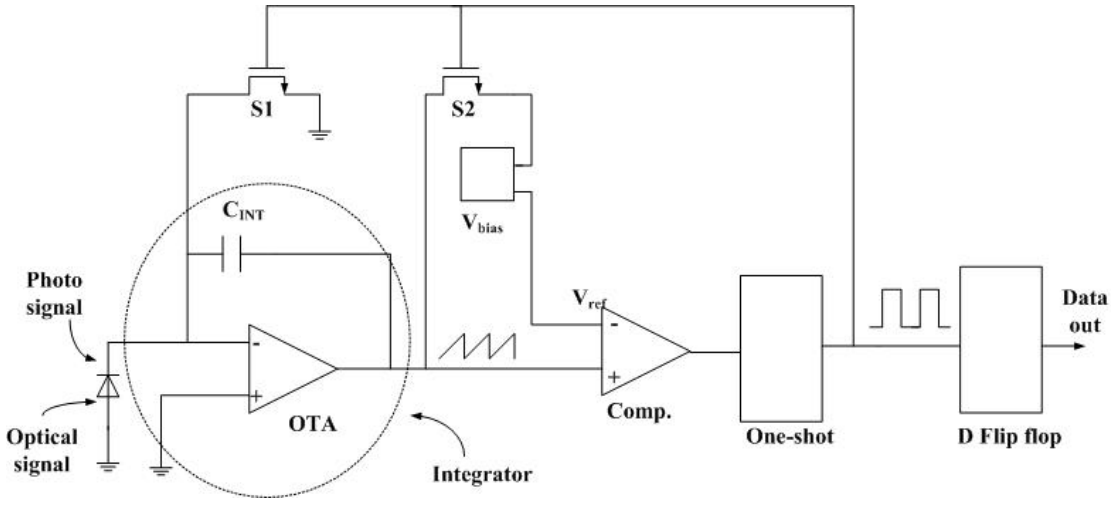

Figure 1.5 Block diagram of the signal processing system [Islam]

1.6 Transmitter

The wireless data transmission is performed by this transmitter system. This integrated wireless transmitter allows for remote sensing without the need for costly cabling to communicate with the sensor. The digital data stream generated by the signal processing circuitry is ASK modulated for transmission. As the BBIC requires low power consumption and only short range communication this simple modulation technique has be chosen.

The direct conversion transmitter used in this design includes a PLL, a mixer and a power amplifier. The PLL is used to generate a 916MHz frequency signal. This signal is mixed with the digital data signal generated from the signal processing circuitry. A doubly balanced Gilbert cell is used to perform the mixing operation. The mixer output is applied to a power amplifier that provides amplification of the RF output power.

This thesis describes the Gilbert cell mixer and the power amplifier circuits designed for the BBIC transmitter system. An insight into the various modulation techniques, transmitter architectures and power amplifiers has been provided in the following chapters.

CHAPTER 2

Modulation Techniques

2.1 Introduction

The Bioluminescent bioreporters integrated circuits (BBICs) consist of the bioluminescent bioreporters, photodiodes and signal processing circuitry. The bioreporters upon exposure to the analyte produce bioluminescence. This light is converted to into a measurable analog electrical signal by the photodiodes. The signal processing circuitry is used to convert the analog electrical signal into a digital pulse stream. A transmitter can be used to send this digital data to a central node for further data collection.

In order to transmit the digital data it is necessary to modulate the incoming data onto a carrier wave. Modulation is defined as a process that causes a shift in the range of frequencies in a signal [Lathi].In order to describe modulation it is necessary to define two types of signals: baseband signal and bandpass signal. A "baseband" signal is defined as the one whose spectral magnitude is nonzero for the frequencies in the vicinity of $\omega = 0$ and negligible elsewhere [Figure 2.1a], for example the signal generated by a microphone or a video camera. A "bandpass" signal is a waveform whose spectral magnitude is nonzero for frequencies in a band around a "carrier" frequency ω_c and negligible outside this band [Figure 2.1b] [Razavi] [Couch].

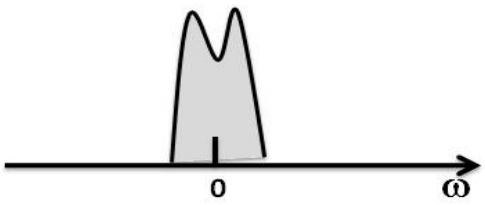

Figure 2.1a Baseband signal [Razavi]

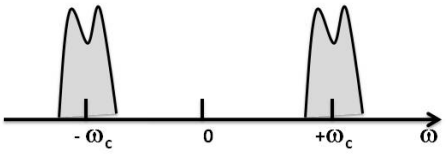

Figure 2.1b Bandpass signal [Razavi]

In general the term "baseband" is used to designate the band of frequencies of the signal delivered by the input source. In telephony, the audio band of 0 to 3.5 kHz represents the baseband. In television, the baseband is the video band occupying 0 to 4.3 MHz. For digital data using signaling at a rate of R_b pulses per second the baseband is 0 to R_b Hz. In baseband communication, the baseband signal is transmitted without any shift in the range of frequencies, that is, without modulation. But long-haul communications over the radio link requires modulation. By performing modulation a baseband signal is converted to its bandpass counterpart. In other words modulation will cause the baseband signal with bandwidth B to occupy a different bandwidth when converted to a bandpass waveform. This communication which uses the modulation to shift the frequency spectrum of the signal is known as carrier communication [Lathi].

The carrier wave is generally considered to be a pure sinusoidal signal, $f_c(\mathrm{t})$. It is called as a carrier wave as it carries the information signal from the transmitter to the receiver.

$$f_c(\mathrm{t}) = \mathrm{A}\cos(\omega_c \mathrm{t} + \theta) \tag{2.1}$$

The baseband signal (information signal or modulating signal), $f(\mathrm{t})$ will be used for varying or modulating one of the parameters of the carrier signal, $f_c(\mathrm{t})$. From the Eq. 2.1 we can find that carrier wave has three parameters that can be varied; the amplitude, A; the angular frequency, ω_c; and the phase, θ. Using the baseband signal to vary the amplitude, the frequency, or the phase leads to amplitude modulation, frequency modulation, or phase modulation respectively.

The modulated signal or bandpass signal can be expressed as,

$$f_m(t) = Re\{ g(t)e^{jw_c t} \} \quad (2.2a)$$

where, Re {.} denotes the real part of {.}, $g(t)$ is called the complex envelope of $f_m(t)$, and f_c is the associated carrier frequency, $\omega_c = 2\pi f_c$. The other equivalent representations are given as,

$$f_m(t) = A(t)\cos[\omega_c t + \theta(t)] \quad (2.2b)$$

and

$$f_m(t) = x(t)\cos\omega_c t - y(t)\sin\omega_c t \quad (2.2c)$$

where

$$g(t) = x(t) + jy(t) = |g(t)|e^{j\angle g(t)} \equiv A(t)e^{j\theta(t)} \quad (2.3)$$

$$x(t) = Re\{g(t)\} \equiv A(t)\cos\theta(t) \quad (2.4a)$$

$$y(t) = Im\{g(t)\} \equiv A(t)\sin\theta(t) \quad (2.4b)$$

$$A(t) \triangleq |g(t)| \equiv \sqrt{x^2(t) + y^2(t)} \quad (2.5a)$$

$$\theta(t) \triangleq \angle g(t) = \tan^{-1}\left(\frac{y(t)}{x(t)}\right) \quad (2.5b)$$

where, $g(t)$, $x(t)$, $y(t)$, $A(t)$, and $\theta(t)$ are all baseband waveforms [Couch].

Here a carrier wave $f_c(t)$ is considered and its amplitude or phase is varied to perform modulation. In the Eq. 2.2b the argument $\omega_c t + \theta(t)$ is called the "total phase" and $\theta(t)$ the "excess phase". The instantaneous frequency is defined as the derivative of the phase: $\omega_c + d\theta/dt$ is the "total frequency" and $d\theta/dt$ is the "excess frequency" or the "frequency deviation" [Razavi].

The inverse of the modulation process is called demodulation or detection. The aim of demodulation is to uniquely recover the information signal from the modulated carrier wave. If the information signal *f(t)* cannot be reproduced accurately at the receiver then modulating it for effective transmission is not of much use. Thus, as shown in Figure 2.2, a simple communication

system consists of a modulator/transmitter, a channel (e.g., air or coaxial cable), and a receiver/detector [Razavi].

2.2 Modulation Techniques

Depending on the baseband signal, the modulation can be either analog modulation or digital modulation. In the case of the BBIC since the data is a digital pulse stream digital modulation techniques are considered.

In digital "RF" systems, a digital baseband signal is used for modulating the carrier signal using some type of generalized modulation techniques. The power spectral density (PSD) for a bandpass signal $f_m(t)$ is given by,

$$P_{f_m}(f) = \frac{1}{4}\ [\,P_g(f - f_c\,) + P_g(-f - f_c\,)] \qquad (2.6)$$

where, f_c is the carrier frequency and $P_g(f)$ is the PSD of the complex envelope [Couch].

The bandpass digital communication systems can be divided into two main categories; binary digital systems and multilevel digital systems. In this thesis the most common binary bandpass signaling techniques will be considered. These are explained below and illustrated in Figure 2.3.

Amplitude-Shift Keying (ASK): It consists of varying the amplitude of the carrier signal. One such case is on-off keying (OOK). It consists of keying (switching) a carrier sinusoidal which is turned *on* and turned *off* with a unipolar binary signal. Morse code radio transmission is an example of this technique.

Binary-Phase Shift Keying (BPSK): It consists of shifting the phase of a sinusoidal carrier 0^o or 180^o with a unipolar binary signal.

Frequency-Shift Keying (FSK): It consists of shifting the frequency of a sinusoidal carrier from a mark frequency (corresponding, for example, to sending a binary 1) to a space frequency (corresponding to sending a binary 0) according to the baseband digital signal [Couch].

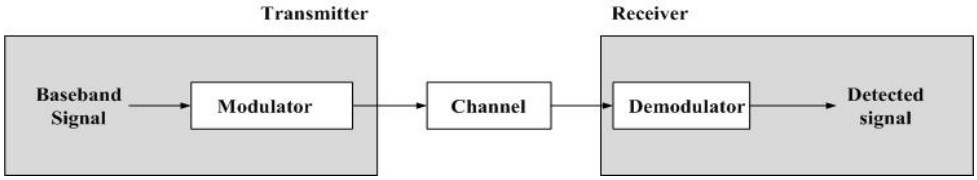

Figure 2.2 A simple communication system [Razavi]

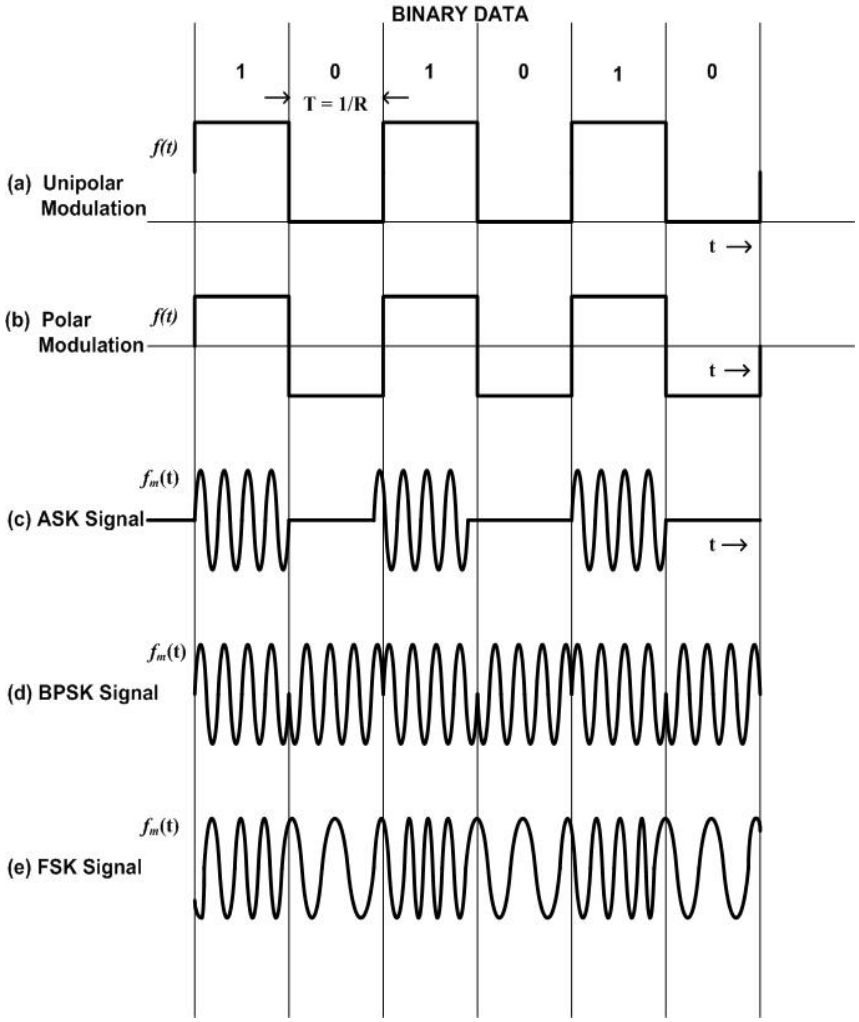

Figure 2.3 Bandpass digitally modulated signals [Couch]

2.2.1 Amplitude-Shift Keying (ASK)

The ASK signal can be represented as shown below,

$$f_m(\mathrm{t}) = \mathrm{A_c}\, f(\mathrm{t}) \cos \omega_c \mathrm{t} \qquad (2.7)$$

where, $f(\mathrm{t})$ is a unipolar baseband digital signal. The complex envelope for ASK is $g(\mathrm{t}) = \mathrm{A_c} f(\mathrm{t})$ and the PSD of this complex envelope is proportional to that for the unipolar signal. It is given by,

$$P_g(f) = \frac{A_c^2}{2}\left[\delta(f) + T_b\left(\frac{\sin(\pi f T_b)}{\pi f T_b}\right)^2\right] \qquad \text{for OOK} \qquad (2.8)$$

where, $f(\mathrm{t})$ has a peak value of $\sqrt{2}$ so that $f_m(\mathrm{t})$ has an average normalized power of $\mathrm{A_c}^2 / 2$.

The PSD for the corresponding ASK signal can be obtained by substituting Eq. 2.8 into Eq. 2.6. The result for positive frequencies is shown in Figure. 2.4. The bit rate is given by R = 1/ $\mathrm{T_b}$. It can be observed that the null-to-null bandwidth is 2R. Therefore the transmission bandwidth of the OOK signal can be given as $\mathrm{B_T}$ = 2B where B is the baseband bandwidth [Couch].

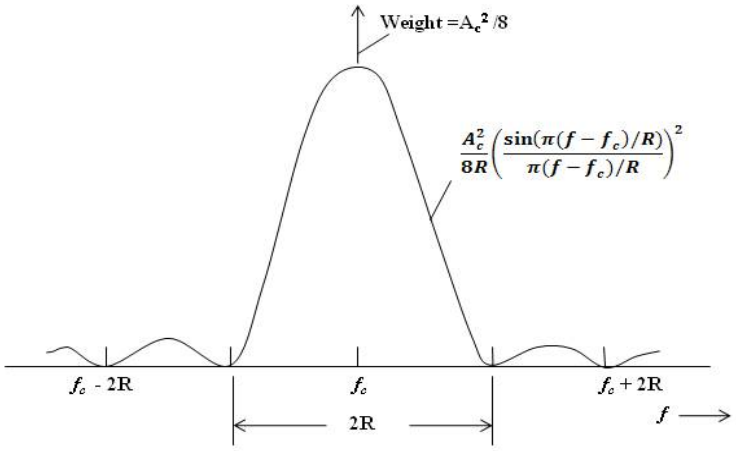

Figure 2.4 PSD of bandpass digital signal for OOK [Couch]

2.2.2 Binary-Phase Shift keying (BPSK)

The BPSK signal is represented as shown below,

$$f_m(\mathrm{t}) = \mathrm{A_c} \cos\left[\omega_c \mathrm{t} + D_p f(\mathrm{t})\right] \tag{2.9}$$

where, $f(\mathrm{t})$ is a polar based baseband digital signal with peak values of ± 1. Eq. 2.9 can be expanded to obtain,

$$f_m(\mathrm{t}) = \mathrm{A_c} \cos\left(\mathrm{D_p} f(\mathrm{t})\right) \cos\omega_c \mathrm{t} - \mathrm{A_c} \sin\left(\mathrm{D_p} f(\mathrm{t})\right) \sin\omega_c \mathrm{t} \tag{2.10}$$

Considering that $\cos(x)$ and $\sin(x)$ are even and odd functions of x, respectively, and $f(\mathrm{t})$ has values of ± 1 the above Eq. 2.10 can be reduced to,

$$f_m(\mathrm{t}) = \left(\mathrm{A_c} \cos \mathrm{D_p}\right) \cos\omega_c \mathrm{t} - \left(\mathrm{A_c} \sin \mathrm{D_p}\right) f(\mathrm{t}) \sin\omega_c \mathrm{t} \tag{2.11}$$

The first term in the Eq.2.11 is called the pilot carrier term and the second term is called the data term. The level of the pilot carrier term is set by the value of $\mathrm{D_p}$ (the peak deviation $\Delta\theta = D_p$). If $\mathrm{D_p}$ is small then the amplitude of the pilot carrier term is relatively large compared to the data term. Thus there will be very little power in the data term which contains the source information. To maximize the signaling efficiency the power in the data term needs to be maximized. This can be achieved by setting $\Delta\theta = 90°$. Then the BPSK signal becomes,

$$f_m(\mathrm{t}) = \mathrm{A_c}\, f(\mathrm{t}) \sin\omega_c \mathrm{t} \tag{2.12}$$

The complex envelope for this signal is $g(\mathrm{t}) = j\mathrm{A_c} f(\mathrm{t})$ and the PSD for the complex envelope is,

$$P_g(f) = A_c^2\, T_b \left(\frac{\sin(\pi f T_b)}{\pi f T_b}\right)^2 \tag{2.13}$$

$f_m(\mathrm{t})$ has an average normalized power of $\mathrm{A_c}^2 / 2$. The PSD for the BPSK signal can be found by substituting Eq.2.13 into Eq.2.6. The result spectrum is shown in Figure 2.5. The null-to-null bandwidth is 2R [Couch].

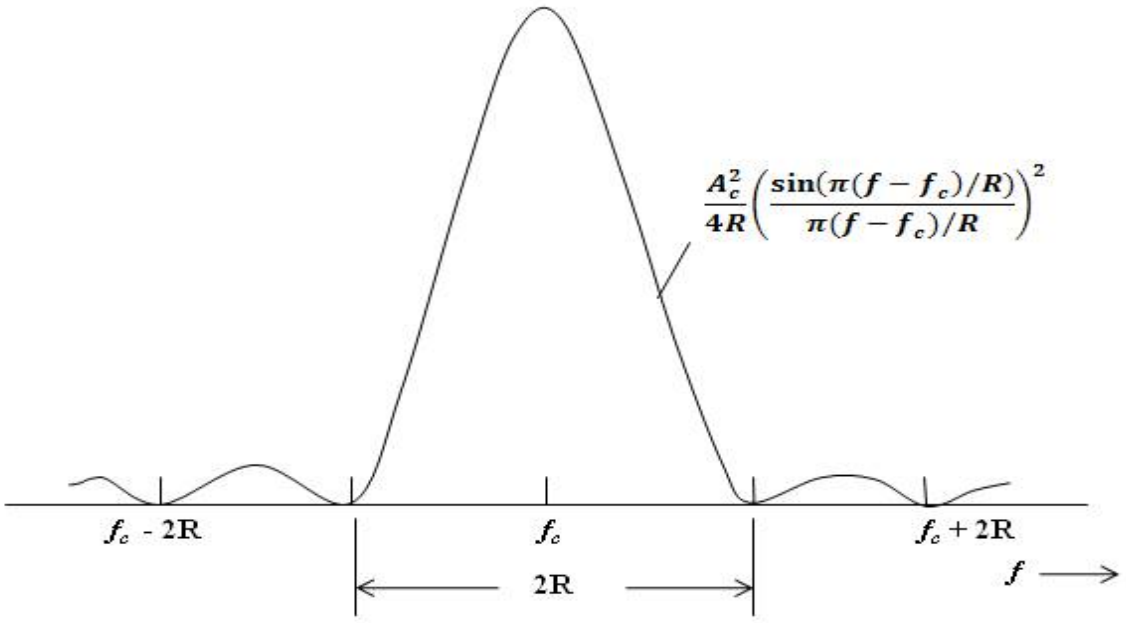

Figure 2.5 PSD of bandpass digital signal for BPSK [Couch]

2.2.3 Frequency-Shift Keying (FSK)

FSK signal can be generated by switching the transmitter output line between two different oscillators as shown in Figure. 2.6a. As this generates an output waveform that is discontinuous at the switching times it is called discontinuous-phase FSK. This can be represented by,

$$f_m(t) = \begin{cases} A_c \cos(\omega_1 t + \theta_1), & \text{for } t \text{ in the time interval when a binary 1 is sent} \\ A_c \cos(\omega_2 t + \theta_2), & \text{for } t \text{ in the time interval when a binary 0 is sent} \end{cases} \quad (2.14)$$

Where, f_1 is called the mark (binary 1) frequency and f_2 is called the space (binary 0) frequency.

The continuous-phase FSK signal can be generated by feeding the data signal into a frequency modulator, as shown in Figure. 2.6b. The resultant signal can be represented by,

$$f_m(t) = A_c \cos\left[\omega_c t + D_f \int_{-\infty}^{t} f(\lambda)\, d\lambda\right] \tag{2.15a}$$

or $$f_m(t) = Re\{g(t)e^{j\omega_c t}\} \tag{2.15b}$$

where, $$g(t) = A_c e^{j\theta(t)} \tag{2.15c}$$

$$\theta(t) = D_f \int_{-\infty}^{t} f(\lambda)\, d\lambda \tag{2.15d}$$

The spectra of the FSK signals are difficult to evaluate since the complex envelope, $g(t)$, is a nonlinear function of $f(t)$[Couch].

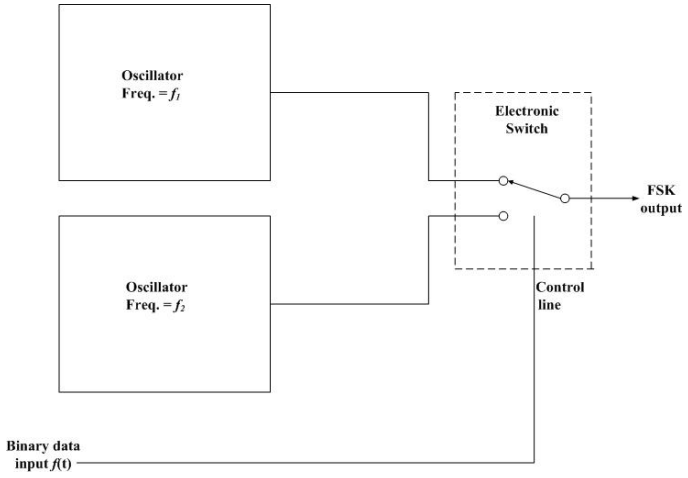

Figure 2.6a Discontinuous-phase FSK [Couch]

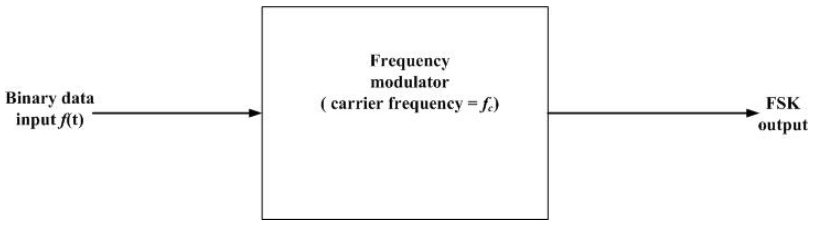

Figure 2.6b Continuous-phase FSK [Couch]

CHAPTER 3

Transmitter System

3.1 Introduction

This chapter initially discusses the various types of transmitter architectures. Then it will examine in detail the Gilbert cell mixer. The various types of power amplifiers are explained followed by the discussion of the power amplifier design.

3.2 Transmitter Architectures

In general, three types of common transmitter architectures are available; super heterodyne, low IF, and direct conversion. Each of these architectures has its own inherent strengths and weaknesses. We will investigate the architectures in the following section.

3.2.1 Super Heterodyne Transmitter

The super heterodyne architecture is sketched in Figure 3.1. The digital baseband signals are passed through the DACs to generate the appropriate I and Q analog baseband signals. These signals are then passed through the low pass filters to reject any high frequency aliasing caused by the DACs. In the example considered here the filtered I and Q signals are passed on to quadrature up-converting mixers running with LO signals at 1.28GHz. They are combined and a single side-band modulated signal is generated at IF (1.28 GHz). The signal is then passed through a band pass filter in order to reduce the spurious signals and to reject any residual DAC aliasing that may have not been completely rejected by the digital and analog baseband filters. The filtered IF signal is then passed through a RF mixer to generate the RF signal at 4.9 to 5.805 GHz depending on the LO frequency. Before passing the signal through a power amplifier, depending on the application another stage of filtering may be applied. The multiple up-conversions result in the use of multiple filters in this architecture. Every time a mixing action takes place one needs to be aware of any image components that may be created.

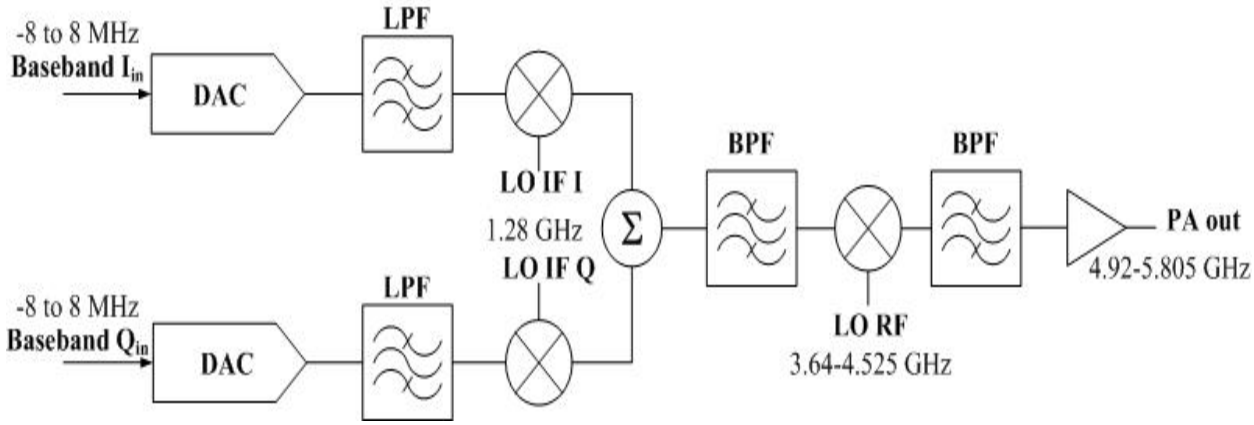

Figure 3.1 Block diagram of super heterodyne 802.11a transmitter [Arya]

The super heterodyne transmitter has a good performance, can achieve very good quadrature balance, can reject extraneous spurs due to extended filtering, and is reasonably low power. On the other hand, this architecture is comparatively large and expensive, has many discrete components and is not suitable for multimode applications due to the narrow band nature of the IF filter [Arya].

3.2.2 Low IF Transmitter

The low IF transmitter works similar to a direct conversion transmitter but it requires full image reject mixers. It has a complex architecture and is seldom used for WLAN applications. This architecture is more popular for narrowband signals. When the low IF architecture is being used, the first stage of up-conversion is to be performed on digital domain so that high degree of image rejection can be maintained.

3.2.3 Direct Conversion Transmitter

An example for this architecture is shown in Figure 3.2. The baseband signals I and Q are passed through the DACs and then through low pass filters to reject any high frequency aliasing caused by the DACs. The filtered signals are then applied to quadrature up-converting mixers. Then the resultant signals are combined and applied to a power amplifier.

This architecture eliminates the IF bandpass filter and the requirements for image filtering and thus offers the lowest overall cost. This architecture provides the highest degree of integration. It can be made to offer high performance and low power consumption. These advantages resulted in choosing this architecture for the BBIC transmitter.

Transmitters generate the modulated signal from the modulating signal $f(\mathrm{t})$ at the carrier frequency f_c. As already mentioned in the previous section the modulated signal can be represented by {Eq. 2.2a, Eq.2.2b, Eq. 2.2c},

$$f_m(t) = Re\{ g(t)e^{jw_c t} \}$$

or,
$$f_m(\mathrm{t}) = \mathrm{A(t)} \cos[\omega_c \mathrm{t} + \theta(\mathrm{t})]$$

and
$$f_m(\mathrm{t}) = x(\mathrm{t}) \cos \omega_c \mathrm{t} - y(\mathrm{t}) \sin \omega_c \mathrm{t}$$

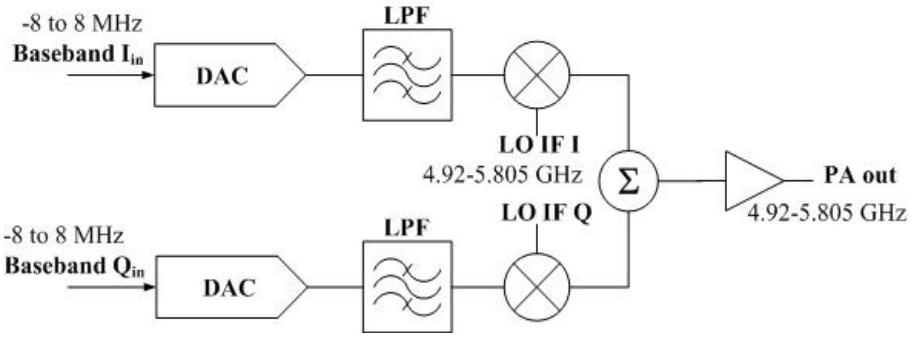

Figure 3.2 Block diagram of direct-conversion transmitter [Arya]

The above two equations can be used to represent the following generalized transmitters using the direct conversion architecture. Eq. 2.2b represents a generalized transmitter using the AM-PM generation technique as shown in Figure. 3.3a. A(t) and θ(t) are generated from $f(t)$ by the baseband signal processing circuit. Nonlinear analog circuits or a digital computer incorporating the A and θ algorithms can be used to implement the signal processing. ADC and DAC are needed in the implementation using a digital computer. As indicated in Figure. 3.3a the remainder of the AM-PM canonical form requires RF circuits.

Figure 3.3b represents the generalized transmitter using the quadrature generation technique. In-phase and quadrature-phase processing is used in this technique. By using analog hardware or digital hardware with software the baseband signal processing may be implemented. As indicated in Figure 3.3b the remainder of the canonical form requires RF circuits [Couch].

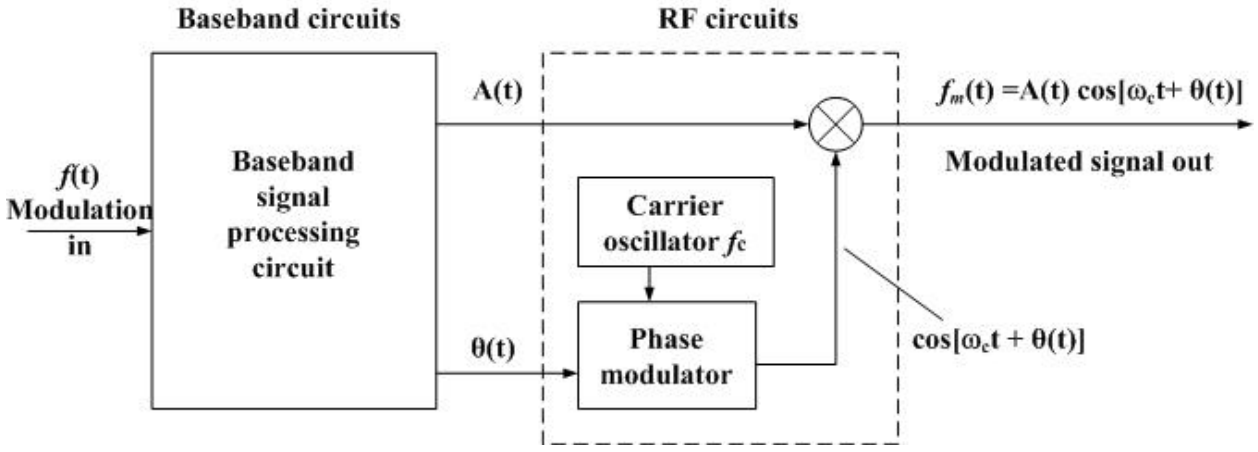

Figure 3.3a Generalized transmitter using the AM-PM generation technique [Couch]

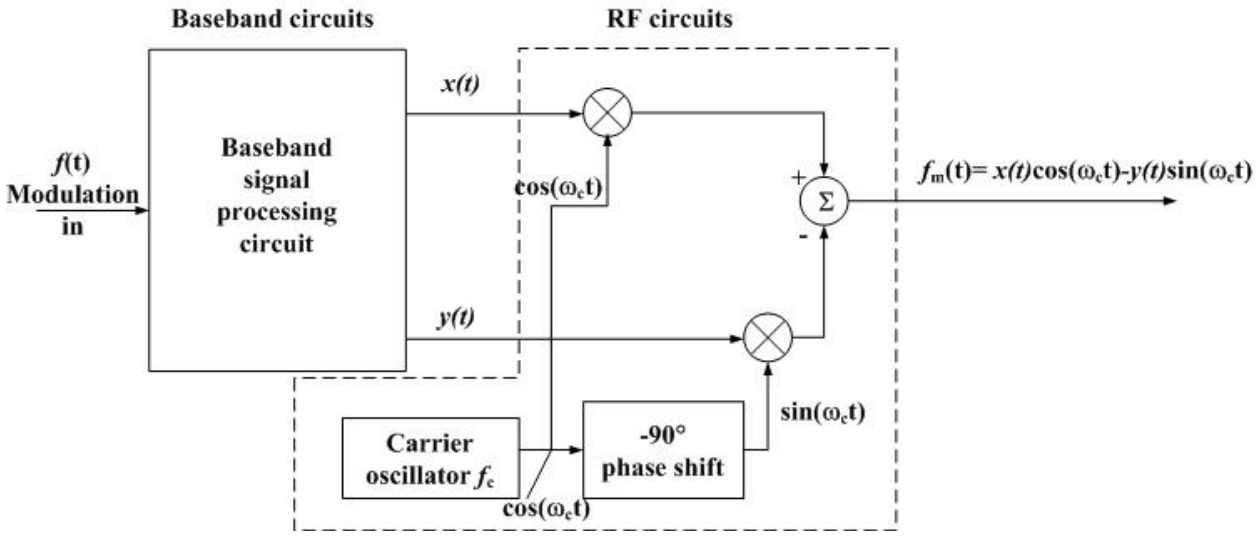

Figure 3.3b Generalized transmitter using the quadrature generation technique [Couch]

The amplitude shift keying is known to be the simplest modulation technique used in data communications. It is not a good choice for long transmission distances as it is not robust enough to prevent the effect of noise during data transmission over long distances. As BBIC requires only short range communication this simple modulation technique has been chosen. Then the AM-PM generation technique showed in Figure 3.3a can be replaced by a more simpler and general transmitter structure as shown in Figure 3.4.

This structure of direct conversion transmitter is made up of a phase locked loop (PLL), a mixer, a power amplifier and an antenna. In Figure 3.4 the data input represents the signal coming out of the signal processing circuitry of the BBIC. This signal is mixed with the 916MHz signal generated by the PLL.

The block diagram of the PLL is shown in Figure 3.5. It includes a crystal frequency reference, a phase/frequency detector, a loop filter, a voltage controlled oscillator and a frequency divider (divided by 256). The phase/frequency detector is used for comparing the phase/frequency difference between the clock signal coming out of the frequency divider and the

frequency reference. Then the charge pump will generate a control voltage for the VCO according to the phase/frequency difference. The loop filter is used to remove the high frequency components of the control voltage and provide a relatively stable one to adjust the frequency of the VCO. The signal frequency from the VCO is divided by 256 by the frequency divider. The PLL has a feedback loop and this makes the output frequency of the VCO stable [Zhang]. This stable frequency is important for the RF transmission and is the input to the mixer. The mixer is an important component of the transmitter and is of primary interest for this work. It is used for multiplying the data signal coming out of the signal processing circuitry of the BBIC with the 916MHz frequency signal generated by the PLL. [Zhang]

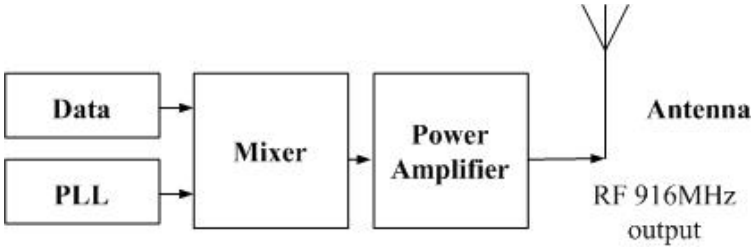

Figure 3.4 Block diagram for a transmitter system [Zhang]

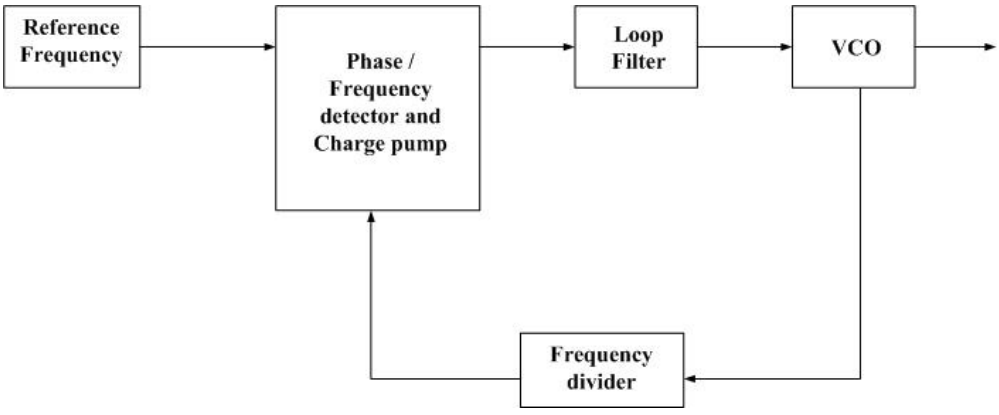

Figure 3.5 Block diagram for phase locked loop (PLL) [Zhang]

3.3 Mixer

The word "mixer" is used to represent both linear and non-linear circuits. The basic linear mixer behaves as a summer circuit. The linear mixer circuit and its schematic are shown in Figure 3.6. Some kind of combiner is needed and as shown, in this case a resistor network is used as a combiner. No interaction occurs between the two input signals F_1 and F_2. Both the signals will share the same pathway at the output, but otherwise do not affect each other. This is similar to the action that one expects of a microphone or other audio mixers [Carr]. The output of the summer is observed on a spectrum analyzer (Figure 3.7) and only the spikes are observed representing the two frequencies and nothing else other than noise.

The non-linear mixer and its schematic are shown in Figure 3.8. While the linear mixer acts as a summer the non-linear mixer behaves as a multiplier. In this case the non-linear element used is a simple diode. The mixing action takes place when the non-linear device exhibits impedance changes over cyclic excursions of the input signals.

The presence of the non-linear element in the signal path results in the generation of a number of new frequencies. If only a single frequency is present, then one can still expect to see its harmonics; for example, F_1 and nF_1 where n is an integer. When more than one frequency is present then a number of product frequencies are generated. The output spectrum for a non-linear mixer is,

$$\pm F_o = mF_1 \pm nF_2 \tag{3.1}$$

where, F_o is the output frequency for a specific (m,n) pair, F_1 and F_2 are the applied frequencies, and m and n are integers or zero (0, 1, 2, 3…)

A unique set of frequencies are generated for each (m, n) ordered pair. These newly generated frequencies are termed as mixer products or intermodulation products. The output observed on the spectrum analyzer is shown in Figure 3.9. Along with the original signals F_1 and F_2, an array of the mixer products arrayed at frequencies away from F_1 and F_2 are present.

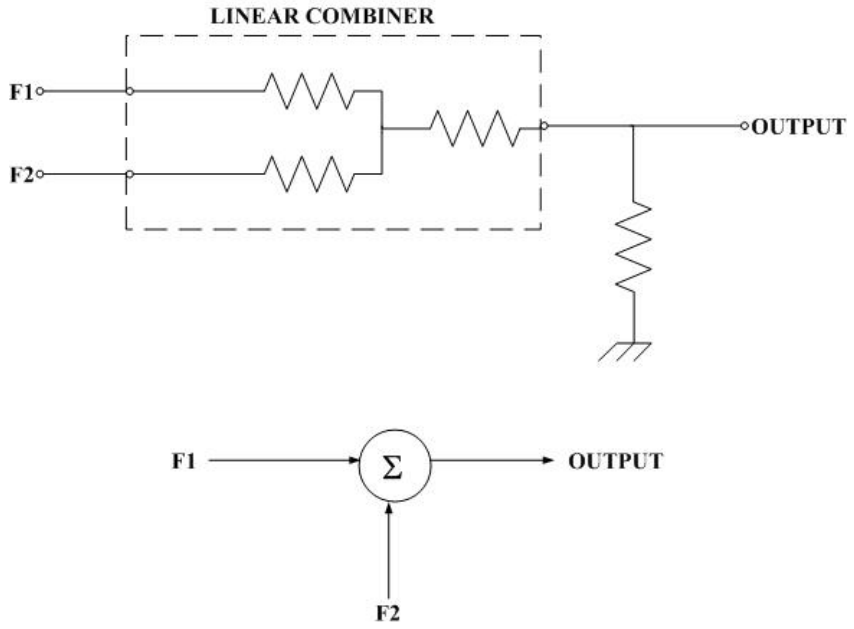

Figure 3.6 Linear combiner (adder) circuit and symbol [Carr]

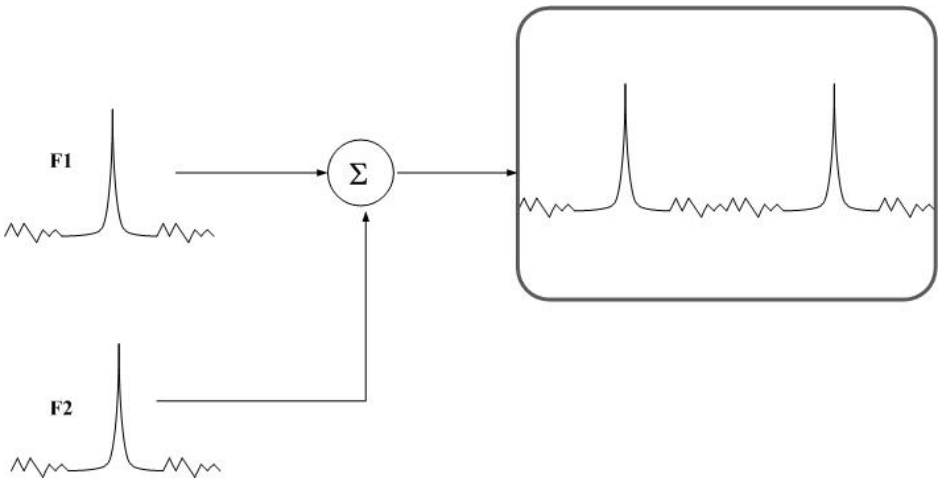

Figure 3.7 Spectrum of adder output [Carr]

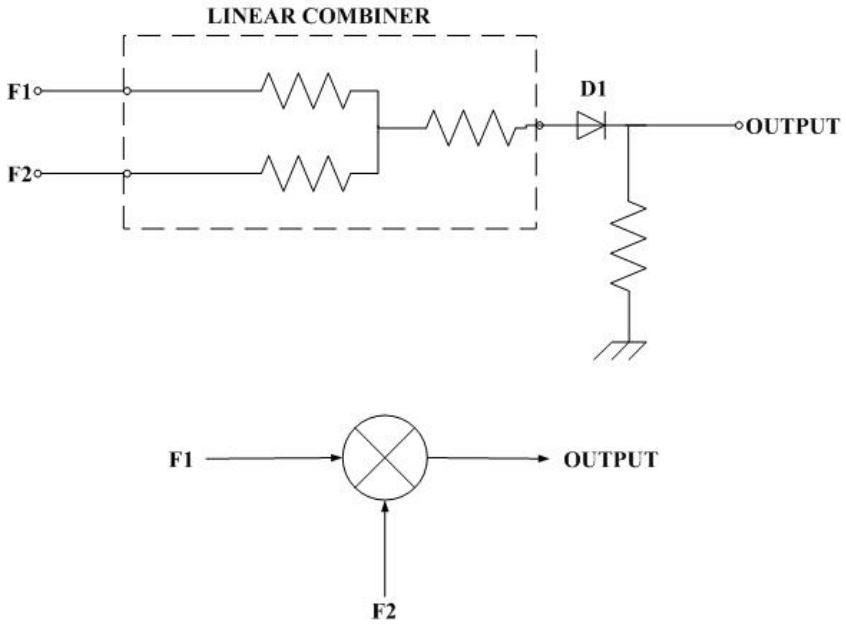

Figure 3.8 Diode mixer circuit and symbol [Carr]

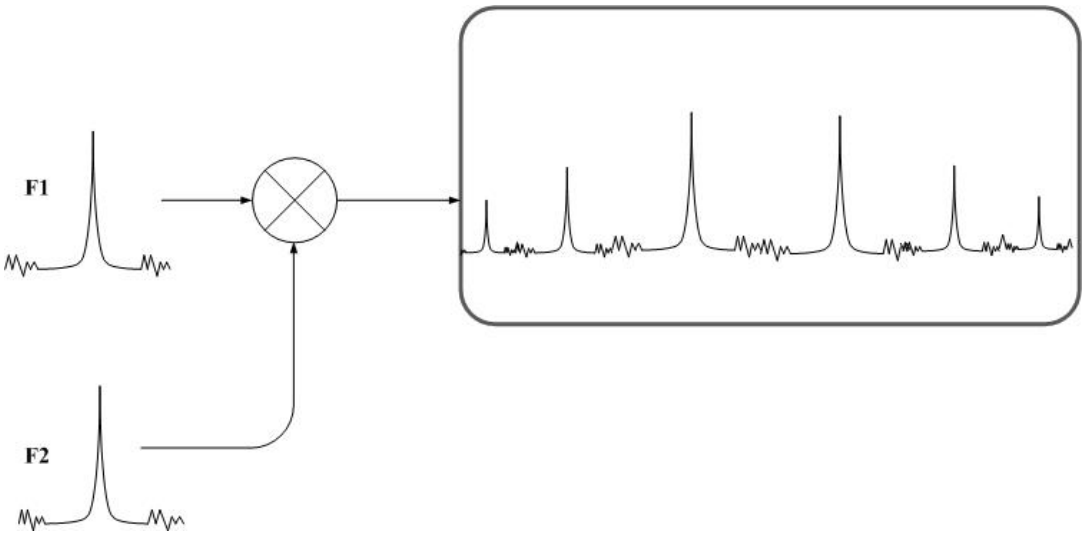

Figure 3.9 Spectrum of mixer output [Carr]

From the Eq 3.1 it can be implied that a number of frequency products are generated of which not all are useful for any specific purpose. Then why does one need to use a mixer? The main purpose of using a mixer is to translate the frequency and in the process transfer the modulation of the original signal. For example, when an AM signal is received, and then translated to a different frequency in the receiver, the modulation characteristics should be essentially undistorted for the AM signal at the new frequency.

Thus a mixer is used for translating the signal spectrum from one frequency to another. In other words a mixer is needed to perform frequency translation. The typical symbol of the mixer is shown in Figure 3.10.

Ideally a mixer should multiply the RF and LO signals to produce the IF signal. It should therefore translate the input spectrum from one frequency to another without any distortion and degradation in noise performance. Most of these requirements can be met by considering the perfect multiplication of two signals as illustrated in the Eq 3.2 below,

$$(V_1 \cos\omega_1 t)(V_2 \cos\omega_2 t) = \frac{V_1 V_2}{2}(\cos(\omega_1 + \omega_2)t + \cos(\omega_1 - \omega_2)t) \qquad (3.2)$$

From the above equation it can be observed that the output which is the product of the two input frequencies consists of the sum and difference frequencies. No other frequency terms than these two are generated and any unwanted signals can be easily removed by filtering.

This mixing is generally achieved by applying the two signals to a non-linear device as mentioned already in the above discussion and as shown in Figure 3.11. The non-linearity can be expressed in the form of Taylor series as in the Eq 3.3 [Jeremy].

$$I_{out} = I_0 + a[V_i(t)] + b[V_i(t)]^2 + c[V_i(t)]^3 + \cdots \qquad (3.3)$$

where, $V_i = V_1 + V_2$

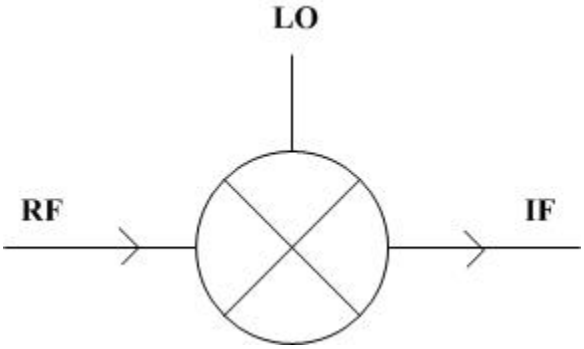

Figure 3.10 Typical symbol for a mixer [Jeremy]

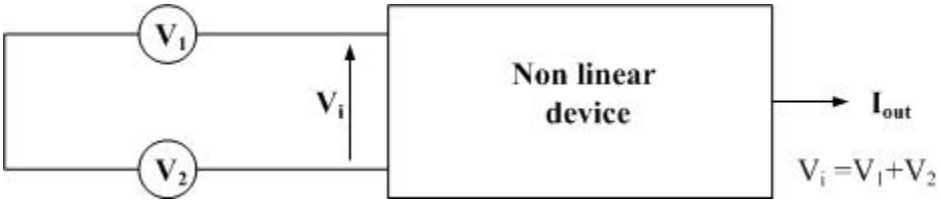

Figure 3.11 Mixing using a non-linear device [Jeremy]

Considering the squared term,

$$b(V_1 + V_2)^2 = b(V_1^2 + 2V_1V_2 + V_2^2) \tag{3.4}$$

It can immediately be observed that the squared term includes a product term and therefore this can be used for the mixing process.

One of the approaches for classifying mixers is whether or not they are unbalanced, single balanced or double balanced.

Unbalanced mixers:

Here both RF and LO signals appear in the output spectrum. They may have poor LO-RF and RF-LO port isolation. Their main attraction is the low cost.

Single balanced mixers:

Here either LO or RF is suppressed in the output spectrum. They also suppress the even-order LO harmonics (2LO, 4LO, 6LO, etc.). High LO-RF isolation is supplied. But external filtering must supply LO-IF isolation.

Double balanced mixers:

In this scheme both LO and RF signals are suppressed in the output spectrum. It even suppresses the even order LO and RF harmonics (2LO, 2RF, 4LO, 4RF, etc.) and high port to port isolation is supplied.

3.3.1 Gilbert Cell Mixer

The Gilbert cell mixer is shown in Figure 3.12. It commutates the RF signals in current instead of in voltage. The transistor M_3 acts as a transconductor and converts the input RF voltage into a current that is passed to the transistors M_1 and M_2. Then the differential pair of transistors M_1 and M_2 commutate the current to the complementary IF outputs for each LO period. As a large swing is not needed between the gates of the differential pair to commutate the current, the requirement of the LO drive gets largely reduced.

There is no direct path from LO to RF and hence better isolation between LO and RF is provided. However, there is still LO leakage into the IF port through the parasitic capacitance present between the gate and the drain of the differential pair transistors. This problem can be solved by using a double balanced Gilbert cell mixer which couples differential LO signals into the same IF output.

A double balanced Gilbert cell mixer is shown in Figure 3.13. The transistors M_3 and M_6 form the differential pair transconductance that converts the RF input voltage into a current. This current is then commutated by the switching action of the transistors $M_1 – M_2$ and $M_4 – M_5$. It can be seen from Figure 3.13 that each side of the IF output is connected with two transistors with 180^o phased LO signals so that the LO leakage from the two transistors cancels each other. That is, the LO feed through from the transistor M_1 will be canceled by that from M_5, and any feed through from M_4 will be canceled by that from M_2.Therefore, only the mixed products of RF and LO will be observed at the IF outputs [Ding].

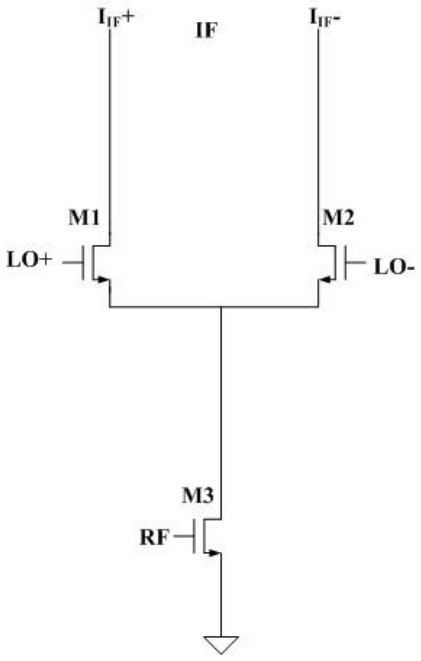

Figure 3.12 Gilbert cell mixer [Ding]

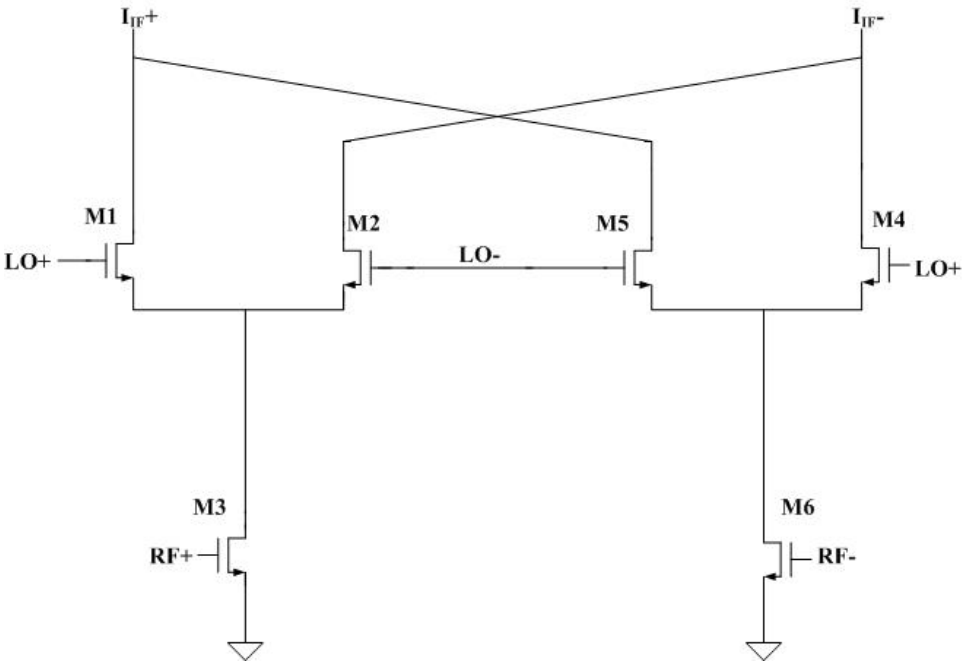

Figure 3.13 Double balanced Gilbert cell mixer [Ding]

3.3.2 Mixer Analysis and Design

The double balanced Gilbert cell mixer used in the design of the transmitter is shown in Figure 3.14. Several design issues must be taken under consideration when designing the Gilbert cell as an up-conversion mixer. The main problem associated with an up-conversion Gilbert cell mixer is the mixer being loaded with PMOS active loads. As the PMOS devices have a lower unity current gain frequency compared to the NMOS devices, the PMOS load devices will limit the maximum operating frequency of the mixer [Sullivan]. The PMOS active loads can be replaced with resistors R_1 and R_2 as shown in Figure 3.14. This adds gain without the frequency limiting effects of the PMOS devices.

The transistors M_7 and M_8 form the RF input differential pair. The RF signal is applied to these transistors which perform the voltage to current conversion. For proper operation of the circuit signals considerably less than the 1dB compression point are used. The transistors M_7 and M_8 are biased to operate in subthreshold region. The drain current in the subthreshold region is dominated by the diffusion mechanism and so it has an exponential dependence on the gate voltage resulting in a higher g_m to I_{DS} ratio. Since this is a low power design it is appropriate to have the transistors operating in subthreshold region as such circuits have a reduced DC power dissipation [Lee].

The digital sensor data of the BBIC is directly up converted to 916MHz to transmit as an ASK message. The digital data is applied to transistors M_3-M_6 which act as switches. The 'local+' input of the mixer i.e., the transistors M_3 and M_6, is tied to V_{DD}. The digital data from BBIC is applied to 'local-'input of the mixer i.e., to the transistors M_4 and M_5. These transistors form the multiplication function, multiplying the RF signal current from the transistors M_7 and M_8 with the digital data LO signal applied across the transistors M_3-M_6 which provide the switching function.

The load resistors R_1 and R_2 form the current to voltage transformation providing the differential output IF signals.

The circuit operation for performing ASK modulation can be explained as follows. The output voltage at the load resistor R_1 depends on the sum of the currents from the transistors M_3 and M_5. The transistor M_3 is always ON as it is tied to $V_{DD.}$ The digital pulse is applied to transistor M_5. When the input to the transistor M_5 is low it is turned OFF. So the current at the output node is entirely from the transistor M_3 as M_5 is OFF. This is converted to a voltage by the load resistor R_1 and results in some output voltage. Now considering the case when the input to transistor M_5 is high, then both the transistors M_3 and M_5 will be ON. Both these transistors will conduct current but the currents are complimentary in nature resulting in a zero output voltage. Thus with the applied digital pulse an ASK modulated output can be obtained.

A simple model of the mixer when operating as an ASK modulator is the load resistors connected directly to the drains of the RF transistors M_7 and $M_{8.}$ Then the circuit is a standard differential amplifier with a voltage gain of g_mR_L. This model, although simple, is not considered to be correct due to the abrupt switching of the transistors M_3-M_6. The actual voltage gain of the mixer is given by,

$$A_V = g_m R_L \left(\frac{2}{\pi}\right) \tag{3.5}$$

where, A_v is the mixer voltage gain, g_m is the transconductance of the differential pair M_7 and M_8, and R_L is the effective load resistance. The above equation can be considered to be a good approximation when the square wave local oscillator voltage driving the transistors M_3-M_6 is large compared to the (V_{gs}-V_t) of the switching transistors M_3-$M_{6.}$ The above equation is the product of the differential voltage gain of the input RF transistors M_7-M_8 and the frequency translated first harmonic of the modulating square wave [Rudell][Arnott].

The RF buffer circuit consisting of the transistors M_1-M_2 and M_{10}-M_{11} is a simple differential source follower amplifier. The reason for using a common source amplifier configuration is its simplicity in implementation, and the circuit also provides a wide band match to the balun transformer [Arnott].

The primary design technique to combat any offsets associated with the differential pairs in the mixer is to use the common centroid geometry for layout of devices in order to minimize the device mismatch due to process variations. Thus to offset any process variations, the transistors M_7, $M_{8,}$ $M_{3,}$ $M_{4,}$ and $M_{5,}$ M_6 are laid out using a common centroid layout technique.

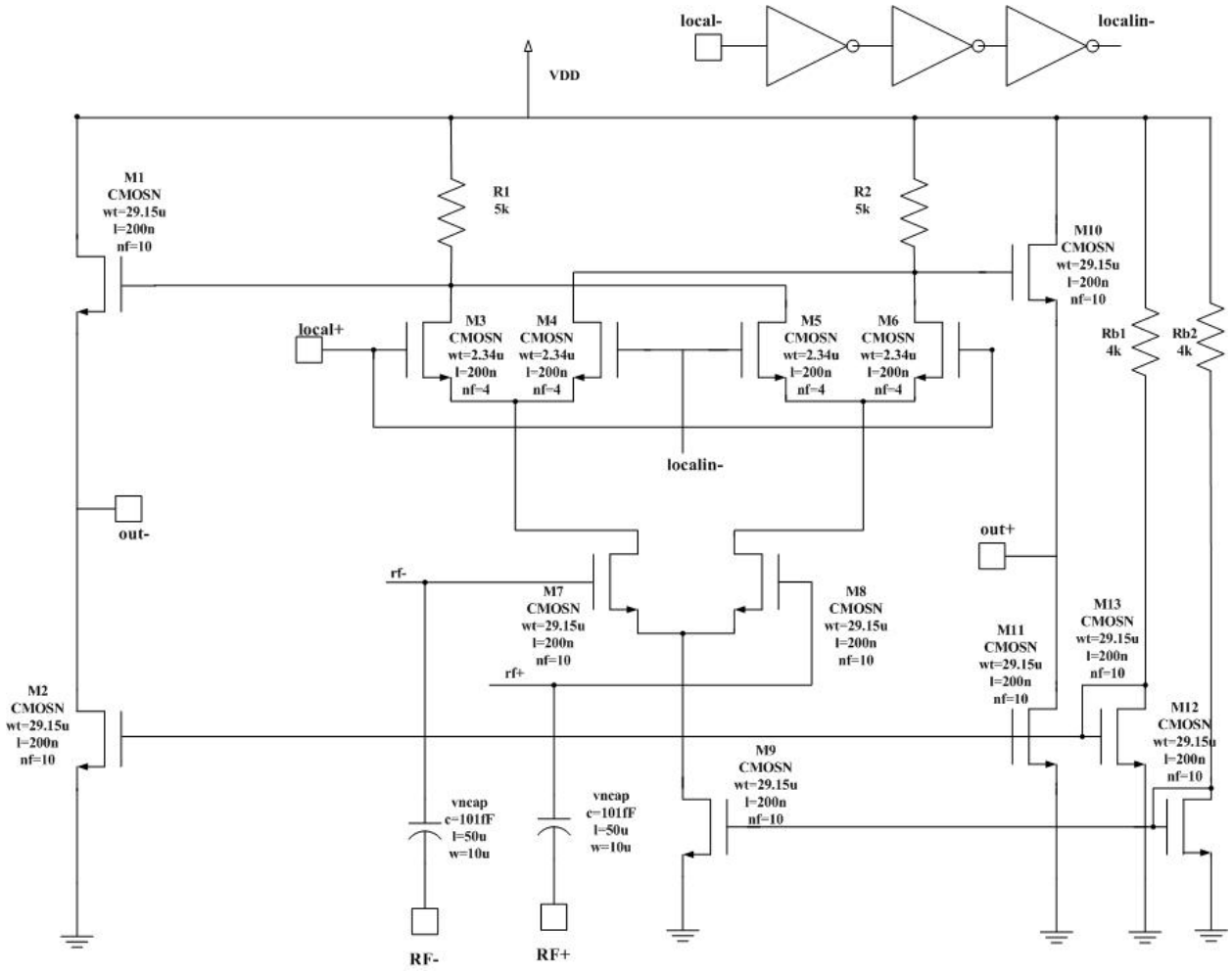

Figure 3.14 Double balanced Gilbert cell mixer

3.3.3 Mixer Bias Circuit

The mixer bias circuit is used to bias the transistors M_7 and M_8 in subthreshold region. The bias circuit is shown in Figure 3.15. It is a simple differential amplifier having a DC feedback loop. It helps to mirror the applied off chip voltage at V_{dc} to the capacitively coupled RF inputs. Figure 3.16 shows the plot where V_{dc} was swept from 0 to 1.2V and the corresponding output was observed. It is clear from the plot that the circuit helps to mirror the applied input voltage. This bias circuit is used to mirror the externally applied 0.7V DC bias level to the mixer RF inputs. The bias circuit is biased to have a current around 40μA which does not increase the power dissipation of the mixer significantly.

Consider Figure 3.17 as shown below. It has three plots with V_{dc} swept from 0 to 1.2V. The x-axis represents V_{dc}. The y-axis of the first plot represents V_{gs} voltage of the RF input transistor M_7. It can be seen from the plot that V_{gs} is around 400mV for a V_{dc} of 0.7V. This is below the threshold voltage and hence the transistor is in subthreshold region. The y-axis of the second plot represents the drain current of M_7 transistor which is around 78 μA for a V_{dc} of 0.7V. The y-axis of the third plot represents the transconductance of M_7 transistor which is around 192 μA/V for a V_{dc} of 0.7V.

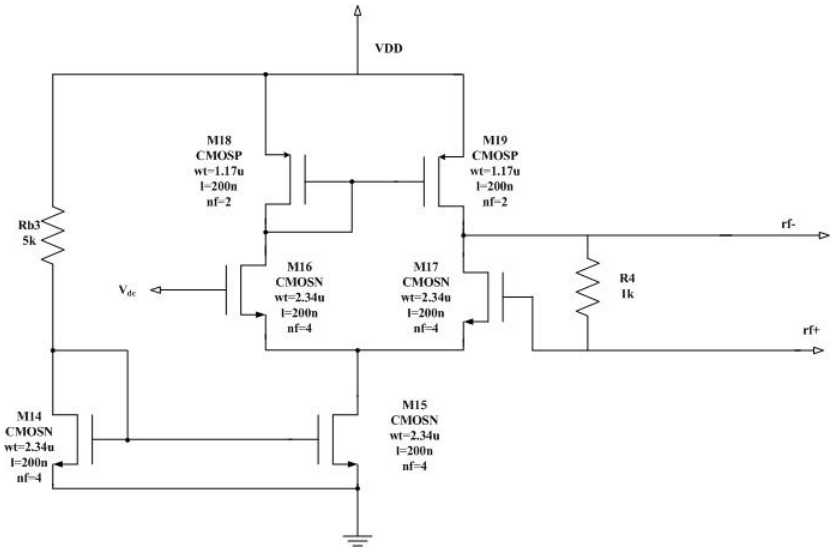

Figure 3.15 Mixer bias circuit

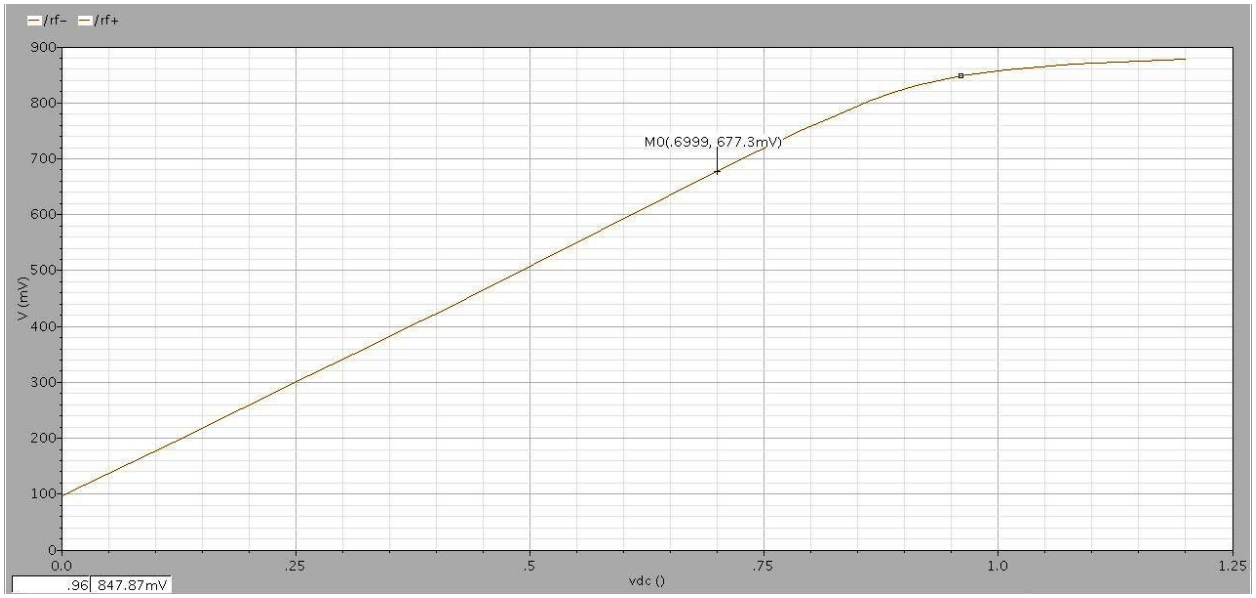

Figure 3.16 Plot showing that the mixer bias circuit mirrors the applied off chip voltage V_{dc}

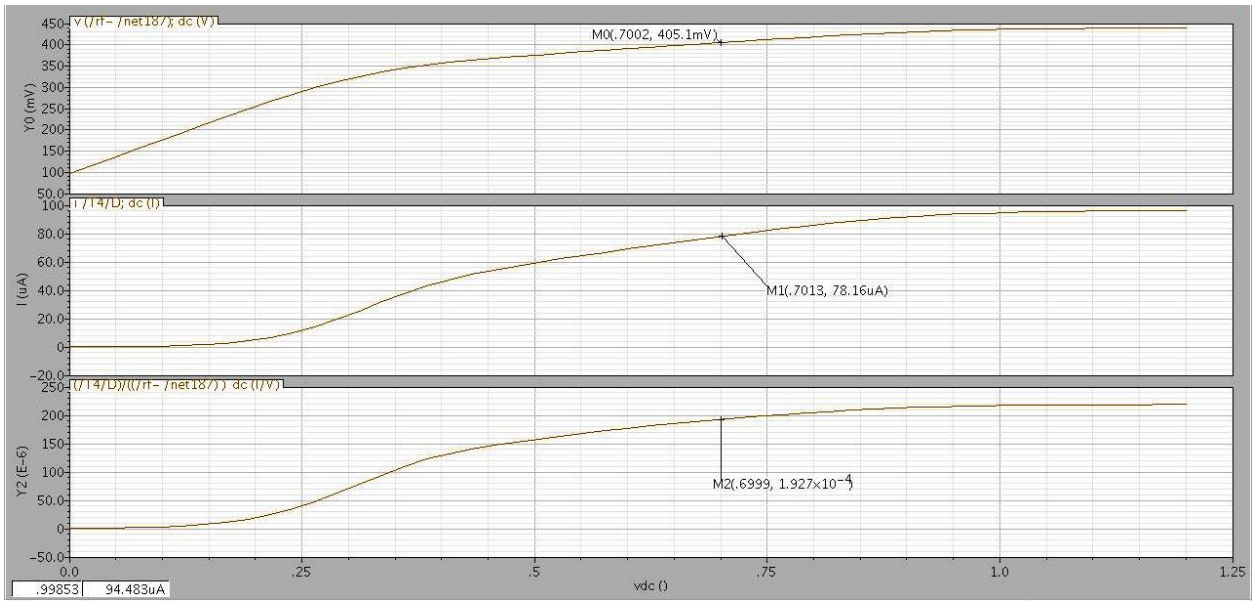

Figure 3.17 Plot showing V_{gs} , drain current and transconductance of RF input transistor M_7 with the mixer bias voltage V_{dc} being swept between 0 and 1.2V

3.4 Power Amplifier

Power amplifier is used for the amplification of the small input RF power to a large output RF power. In this work power amplifier can be considered as an amplifier which has been optimized in terms of its ability to deliver power to a load in an efficient manner.

3.4.1 Efficiency and Gain

The important power amplifier performance metrics are efficiency and gain. Efficiency describes how well an amplifier can convert DC input power to RF output power. This is referred to as the DC-to-RF power conversion efficiency. More often this is referred to as the drain efficiency. Drain efficiency can be defined mathematically as the ratio of the average RF output power to the DC input power.

$$DE = \eta = \frac{P_{OUT,RF}}{P_{IN,DC}} \tag{3.6}$$

Gain refers to how well an amplifier can convert input RF power to output RF output power. Power gain can be defined as the ratio of the average RF output power to the average RF input power.

$$G = \frac{P_{OUT,RF}}{P_{IN,RF}} \tag{3.7}$$

3.4.2 Power Added Efficiency

The quantity that characterizes an amplifier's power gain and drain efficiency is known as the power added efficiency (PAE). It is defined as the RF output power minus the RF input power divided by the DC supply power.

$$PAE = \frac{P_{OUT,RF} - P_{IN,RF}}{P_{IN,DC}} \tag{3.8}$$

It can also be re-written as,

$$PAE = DE\ (1 - \frac{1}{G}) \tag{3.9}$$

From the Eq. 3.9 it can be clearly seen that PAE depends on power gain and drain efficiency. As the power gain becomes very large, the PAE approaches the drain efficiency.

3.4.3 Gain Compression

The amplifier's deviation from its ideal linear gain curve refers to gain compression. 1-dB gain compression point is generally used for the characterization of the amplifiers. The 1-dB compression point can be defined as the point of the input-output transfer characteristics where the actual gain is 1-dB below the ideal liner gain. It represents an arbitrary upper limit of the input signal for which the amplifier approximates the linear operation. This condition is shown in Figure. 3.18.

3.4.4 Total Harmonic Distortion

Total harmonic distortion (THD) is a very common method used for characterizing an amplifier's non-linearity. If the input to the amplifier is a single tone, a cosine wave signal $\cos(\omega_0 t)$, then the output will be:

$$V_{OUT} = a_0 + a_1 \cos(\omega_0 t) + a_2 \cos(\omega_0 t)^2 + a_3 \cos(\omega_0 t)^3 + \ .... \qquad (3.10)$$

Since raising a cosine of frequency ω_0 to a power n will create a harmonic at a frequency $n\omega_0$ plus other spectral components, therefore, the degree of non-linearity of an amplifier can be characterized by the analyzing the spectral components in the output signal, when the input is driven by a clean sine wave. This test is the basis for the measurement of THD. The THD is given as,

$$THD = \frac{\Sigma P_{Harmonics} - P_{Fundamental}}{P_{Fundamental}} \qquad (3.11)$$

where, $\sum P_{Harmonics}$ is the total signal power and $P_{Fundamental}$ is the total fundamental signal power.

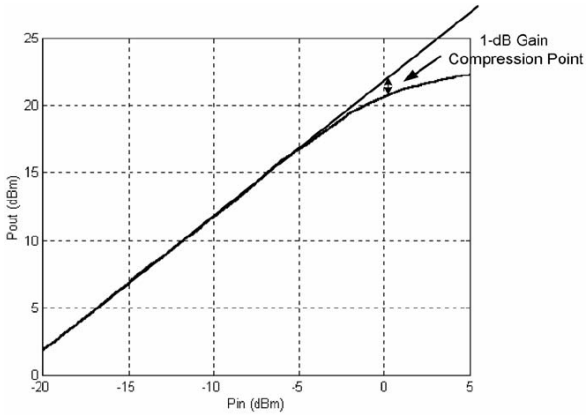

Figure 3.18 Pout vs. Pin plot for a generic linear amplifier [Terry]

3.5 Current Source Power Amplifiers

An amplifying device is said to be a current source power amplifier when it operates only in saturation and in cut-off. A circuit topology that can be used to realize any current source power amplifier is shown in Figure. 3.19. The important current and voltage waveforms associated with the amplifier are also shown in Figure. 3.19. Common source configuration is used as it yields the highest efficiency of all the common amplifier configurations. The drain bias is provided to the amplifier by using an RF choke. The RF choke acts as a nearly ideal DC current source. It dissipates only nominal power and can withstand positive and negative voltages. Finally the output signal is AC-coupled into a resonant tank which is used to reduce the harmonics present in the output signal. The conduction angle is given as,

$$conduction \angle = 360° \left(\frac{T_{ON}}{T_{RF}}\right) \tag{3.12}$$

where, T_{ON} is the time during which the active device conducts current, and T_{RF} is the period of the RF cycle. The conduction angle can be increased or decreased by simply increasing or decreasing the average and/or the peak value of the input signal. For this case the conduction angle is 360^{o}, as evident from the transistor current waveforms. The inductor L_{DC} will have ideally a zero voltage drop. Therefore an AC signal on the drain must have a mean value of V_{dd}. The final output voltage has no DC offset due to the presence of the blocking capacitor.

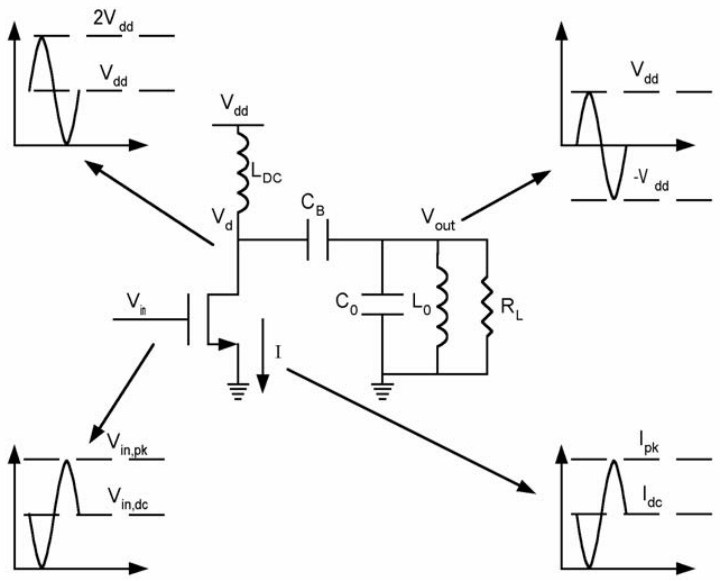

Figure 3.19 Basic topology for a current source power amplifier [Terry]

3.5.1 Class A Power Amplifier

The term Class A power amplifier can be used interchangeably with the term linear amplifier. In reality, Class A power amplifier is the one in which the transistor conducts current for the entire 360^o of the input cycle, and is not necessarily linear. However Class A power amplifier exhibits non-linearities because it has to sustain a large current and voltage swing. The transistor current and voltage waveforms are shown in Figure 3.20.

The maximum efficiency will occur when the drain voltage swings from 0 to $2V_{dd}$. The input power is given by,

$$P_{in,dc} = V_{dd} I_{dd} = \frac{V_{dd}^2}{R_L} \tag{3.13}$$

The output power is given by,

$$P_{out,RF} = \frac{V_{dd}^2}{2R_L} \tag{3.14}$$

Finally the drain efficiency can be calculated as,

$$DE = \frac{V_{dd}^2/2R_L}{V_{dd}^2/R_L} = \frac{1}{2} \tag{3.15}$$

3.5.2 Class B Power Amplifier

The main drawback of Class A amplifier is that the active device dissipates significant power compared to the peak RF output power. The active device can be biased such that it conducts current for less than a full RF cycle so that the power dissipation can be reduced. In other words one can drive the device into cutoff for some portion of the RF cycle. The Class B power amplifier is biased to conduct current for only one-half of the RF cycle. The harmonics are reduced using the tank circuit loading the amplifier. The current and voltage waveforms are shown in Figure 3.21. It can be seen that the drain current is only half of a sine wave.

The DC bias current can be found as the average value over one RF cycle of one half of a sine wave,

$$I_{dd} = \frac{1}{T_0}\int_0^{\frac{T_0}{2}} \sin\left(\frac{2\pi}{T_0}.t\right) dt = \frac{2}{\pi}\frac{V_{dd}}{R_L} \tag{3.16}$$

and the drain efficiency can be calculated as,

$$DE = \frac{V_{dd}^2/2R_L}{2\left(V_{dd}^2/\pi R_L\right)} = \frac{\pi}{4} \cong 0.785 \tag{3.17}$$

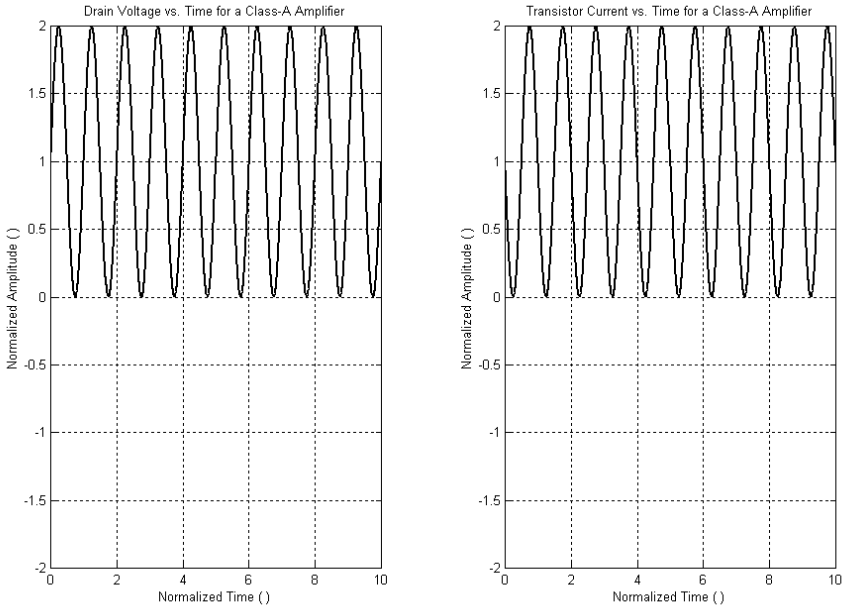

Figure 3.20 Class-A amplifier waveforms [Terry]

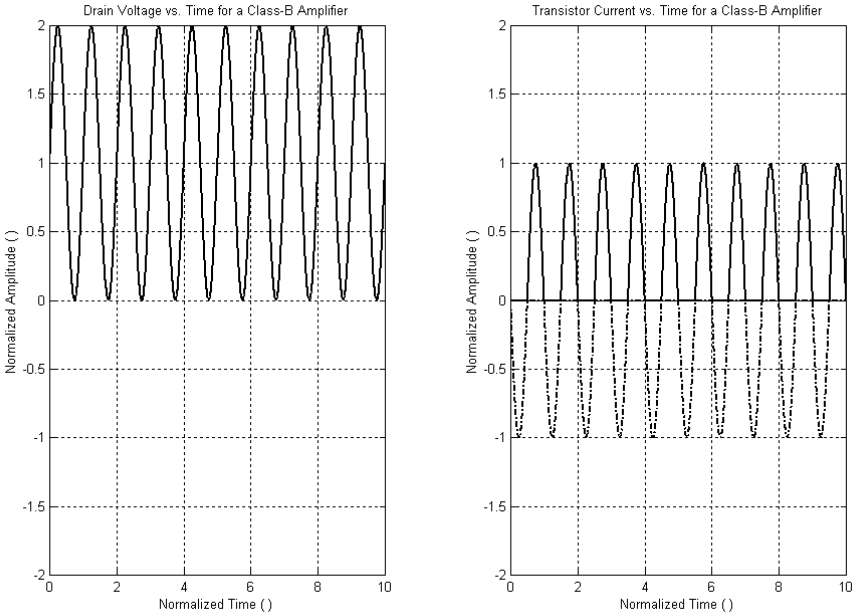

Figure 3.21 Class-B amplifier waveforms [Terry]

3.5.3 Class A-B Power Amplifier

Class B power amplifier trades efficiency for linearity. However it is desirable to have an amplifier with better efficiency than the Class A amplifier, and better linearity than the Class B amplifier. These specifications are met by Class A-B amplifier. The conduction angle for this is somewhere between 180^o and 360^o. The efficiency lies between 0.5 and 0.785. The waveforms are shown in Figure 3.22. The conduction is halfway in between Class A mode and Class B mode.

3.5.4 Class C Power Amplifier

The previously discussed amplifiers can be used as linear amplifiers. But in applications where efficiency is a priority Class C amplifier can be used. It has a conduction angle less than 180^o and can achieve efficiencies greater than Class B amplifier. The transistor waveforms are shown in Figure 3.23.

The theoretical maximum efficiency is a function of the conduction angle and is given by,

$$\eta_{max} = \frac{2y - sin2y}{4(siny - ycosy)} \tag{3.18}$$

The efficiency can be increased arbitrarily towards unity. The parameter *y* is equal to the conduction angle expressed as a percentage of the RF period.

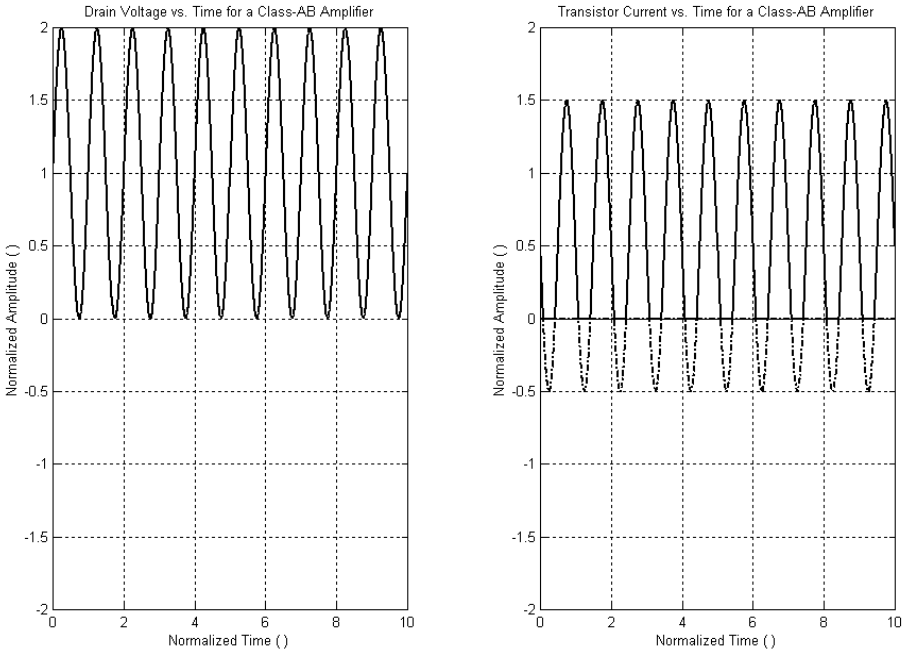

Figure 3.22 Class-AB amplifier waveforms [Terry]

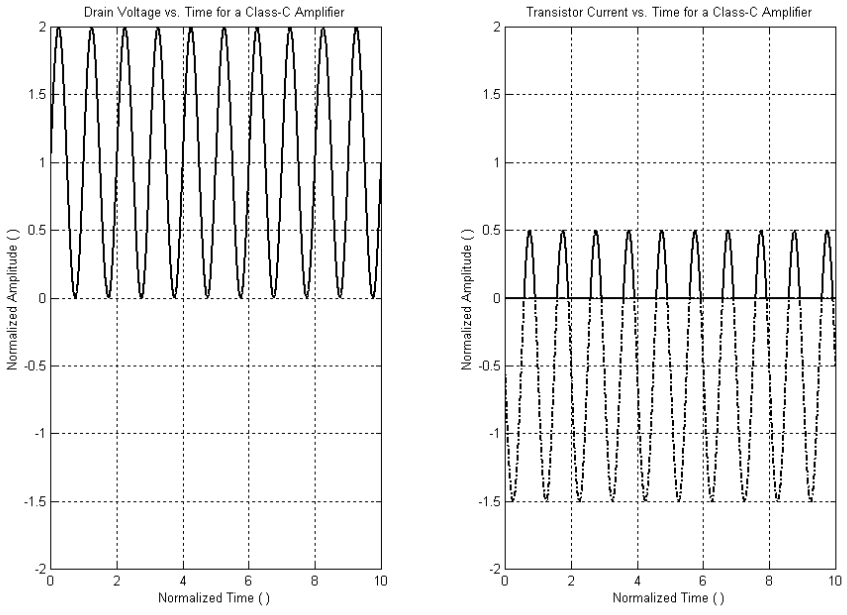

Figure 3.23 Class-C amplifier waveforms [Terry]

3.6 Power Amplifier Design

The power amplifier considered in this BBIC design is a Class A power amplifier. Although the efficiency is less compared to other amplifiers this amplifier was chosen for its simplicity. As it is a Class A amplifier it operates for the entire 360° of the input cycle. The output signal will also have the entire 360° phase like the input signal.

The schematic of the power amplifier is shown in Figure 3.24. N_0 and N_1 transistors provide the two stage amplification. The gate voltages of N_0 and N_1 are biased to about 1V and the transistors operate in saturation region. The second harmonic distortion in the output signal will be reduced by L_2 and C_2 which offer very high impedance to any second harmonic currents.

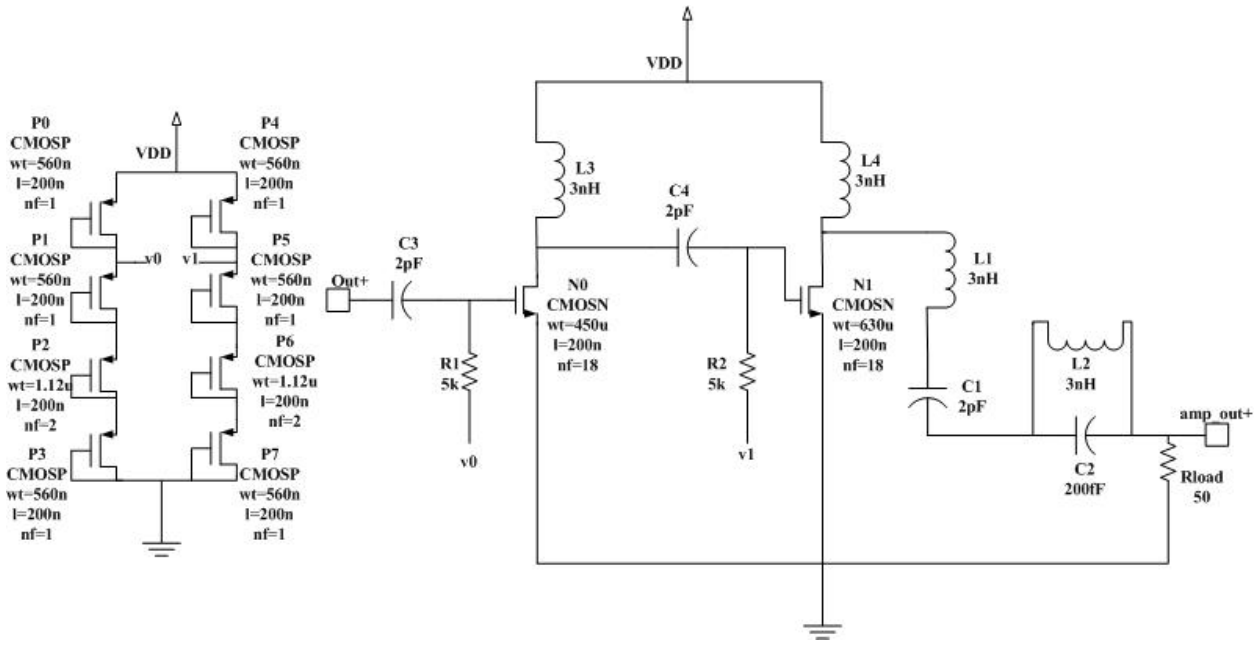

Figure 3.24 Power amplifier

CHAPTER 4

Simulation and Test Results

4.1 Mixer Simulation Results

The mixer has been simulated using Cadence Spectre. As a first step the DC analysis was performed to make sure the transistors were biased in the correct region of operation. Then a -20 dBm differential sinusoidal signal of 916 MHz has been applied to a balun. The balun was used to convert the single ended unbalanced input to differential balanced signals that were applied to the gates of the RF input transistors. Although the digital BBIC data signal is around 1 kHz, a much higher frequency of 10 MHz has been used to expedite the simulation. A 10 MHz square wave with amplitude varying between 0 and 1.2 V has been applied to the 'local-'input of the mixer. The 'local+' input of the mixer has been connected to V_{DD} of 1.2V. A bias voltage of 0.7V for the mixer bias circuit has been applied to the V_{dc} input. Figure 4.1 shows the test bench setup for the mixer simulation.

The following simulations were performed and the results are shown below.

1. The transient analysis has been performed and the resultant output was observed to be ASK modulated. The ASK modulated output is shown in Figure 4.2.

2. The mixer's power gain and voltage gain were simulated. A power gain of 7.31dB was obtained and the voltage gain was measured to be 0.15V/V at an output harmonic of 926 MHz. The power gain and the voltage gain are shown in Figure 4.3 and Figure 4.4, respectively.

3. The 1-dB compression point was measured along with the average power consumption. Figure 4.5 shows the input referred 1-dB compression point which is observed to be around -10dBm at the output frequency of 926 MHz. The input referred IP3 value of -657mdBm was obtained by performing a two tone analysis and is shown in Figure 4.6. The average power consumption was 14.1mW.

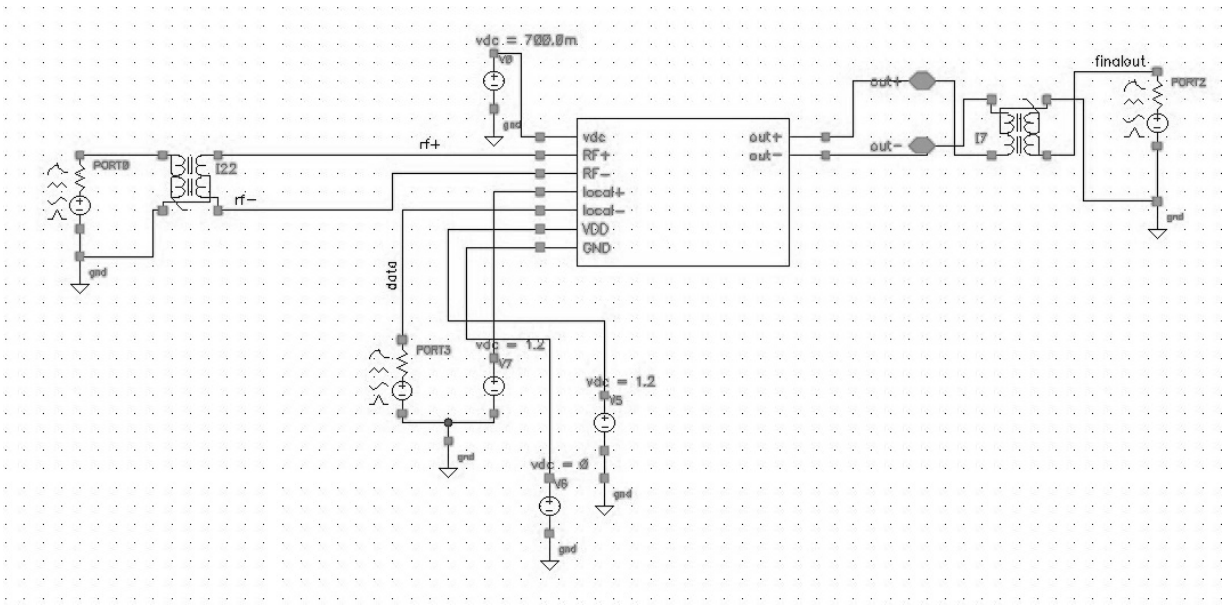

Figure 4.1 Test bench setup for the simulation of mixer

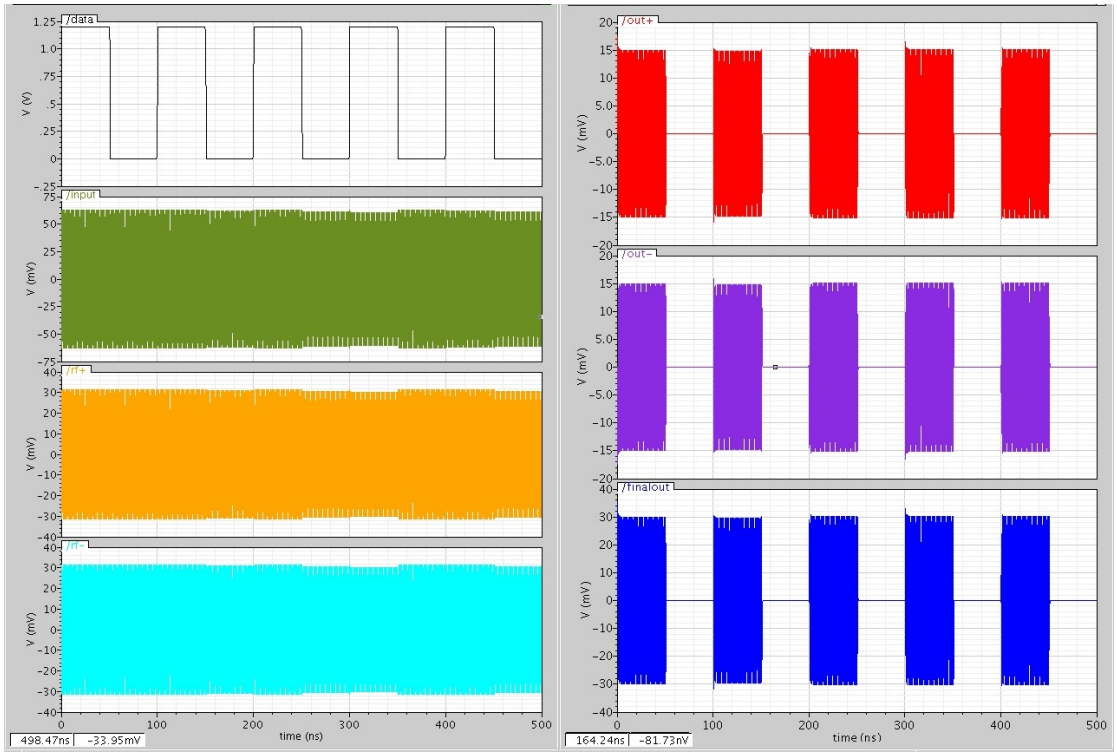

Figure 4.2 ASK modulated output obtained by performing transient analysis on the mixer

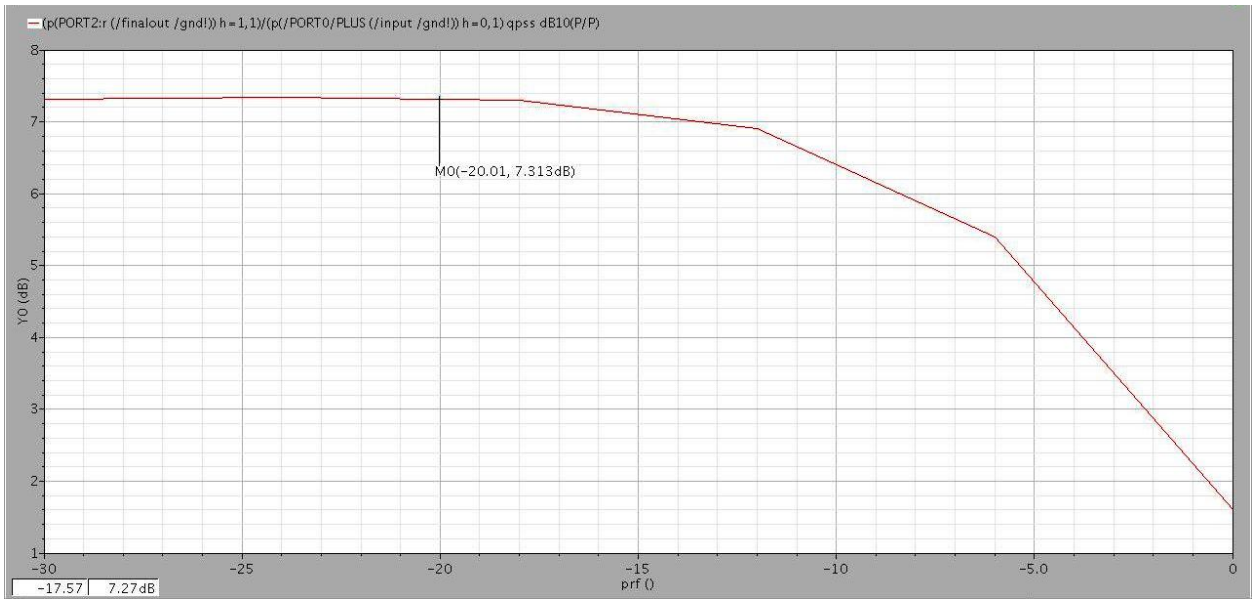

Figure 4.3 Power gain of the mixer

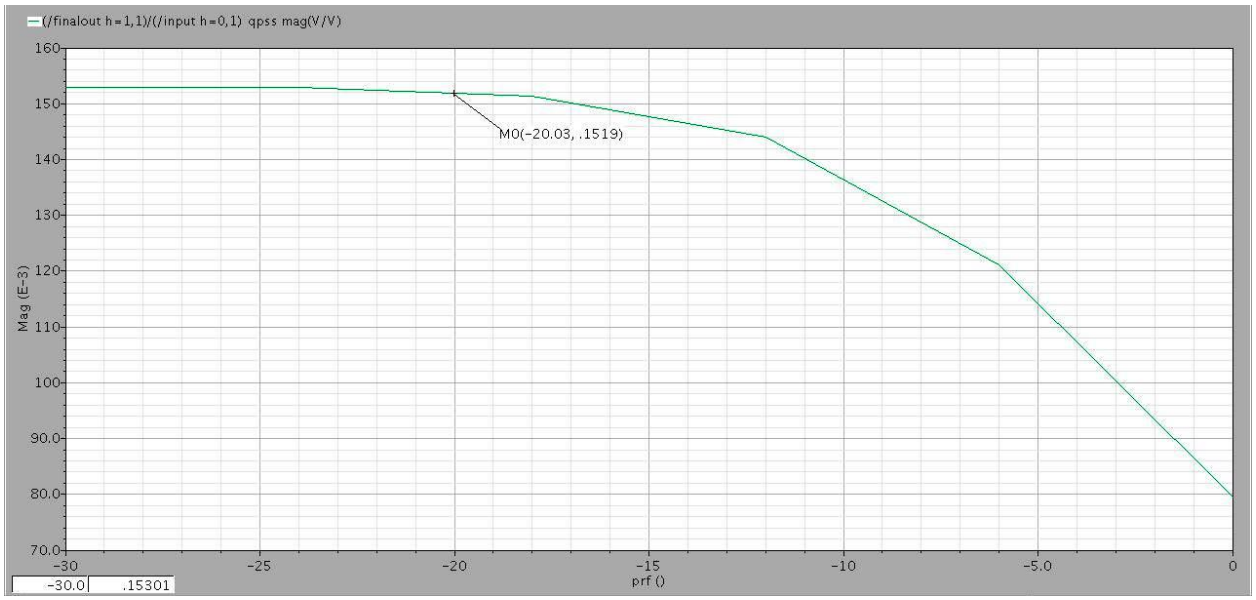

Figure 4.4 Voltage gain of the mixer

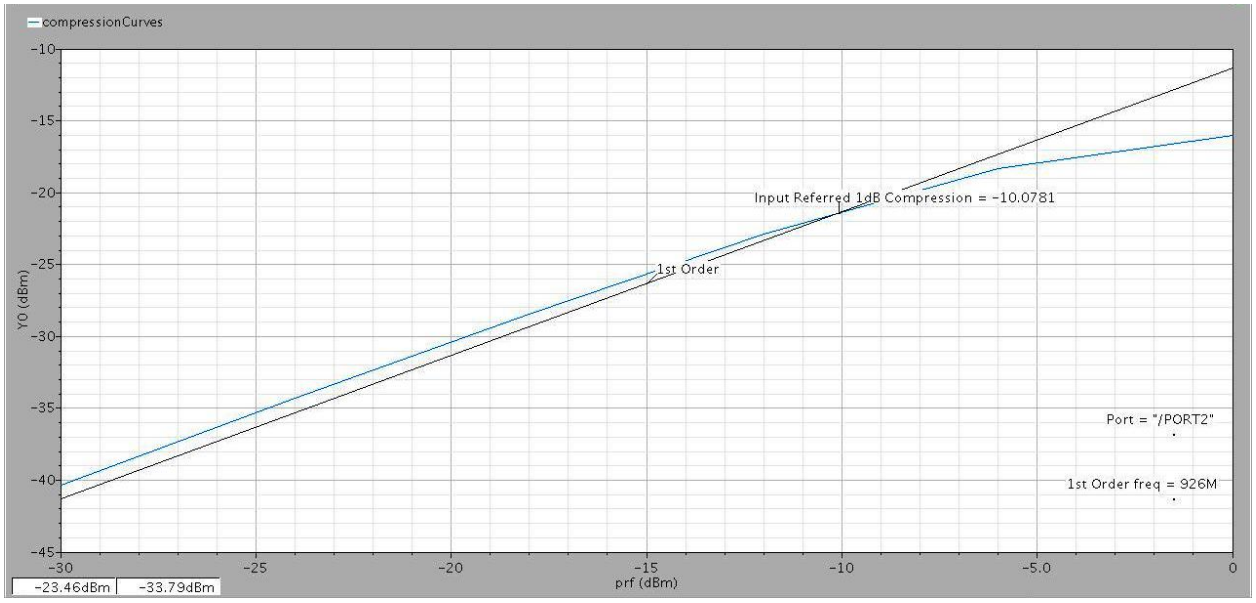

Figure 4.5 1-dB Compression point of the mixer

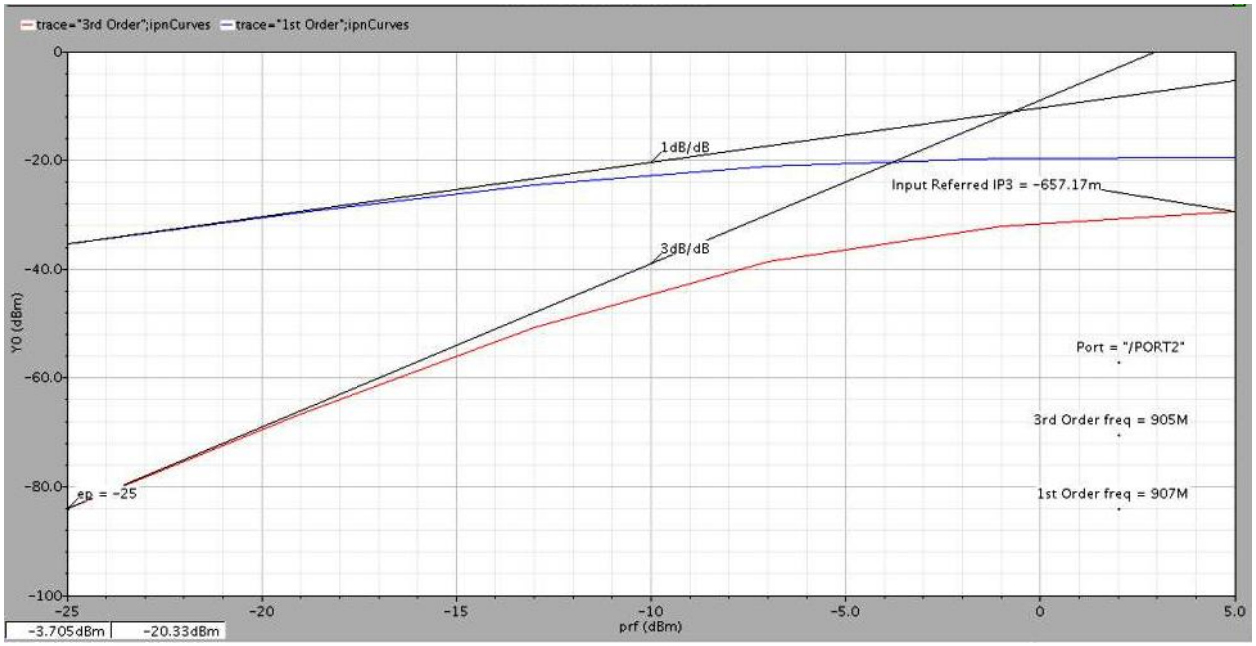

Figure 4.6 IP3 value of the mixer

4.2 Power Amplifier Simulation Results

The power amplifier test bench is shown in Figure 4.7. A -20dBm sinusoidal signal of 916MHz is applied at the input port. A power gain of 24dB was obtained as shown in Figure 4.8. Figure 4.9 shows the voltage gain which is 2.24V/V. The input and output referred 1-dB compression points of -26dBm and -12dBm were observed as shown in Figure 4.10. The input and the output referred IP3 values are shown in Figure 4.11. A significant power consumption of 300mW was observed as it is a Class A power amplifier.

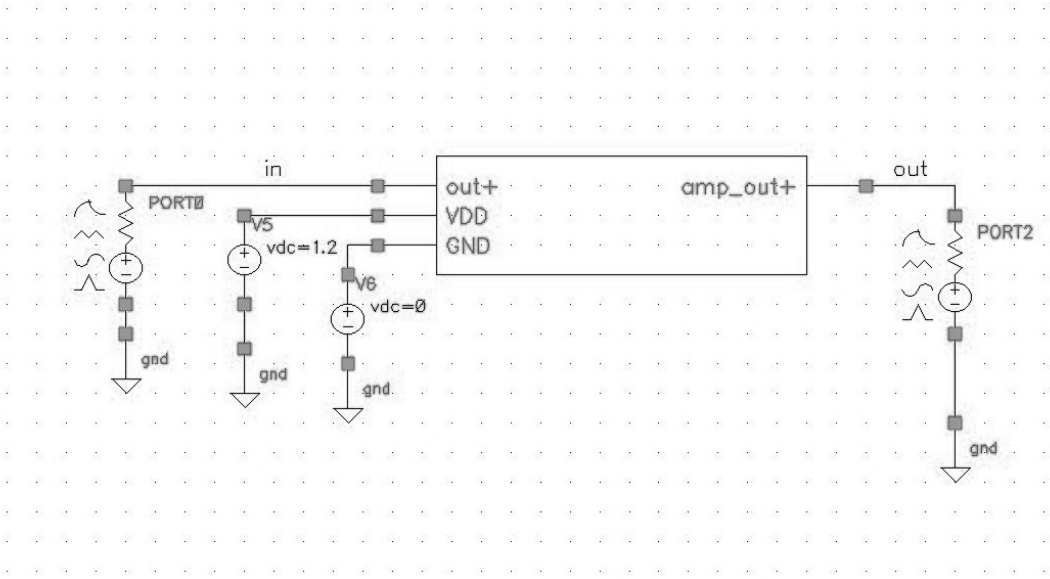

Figure 4.7 Test bench setup for simulation of power amplifier

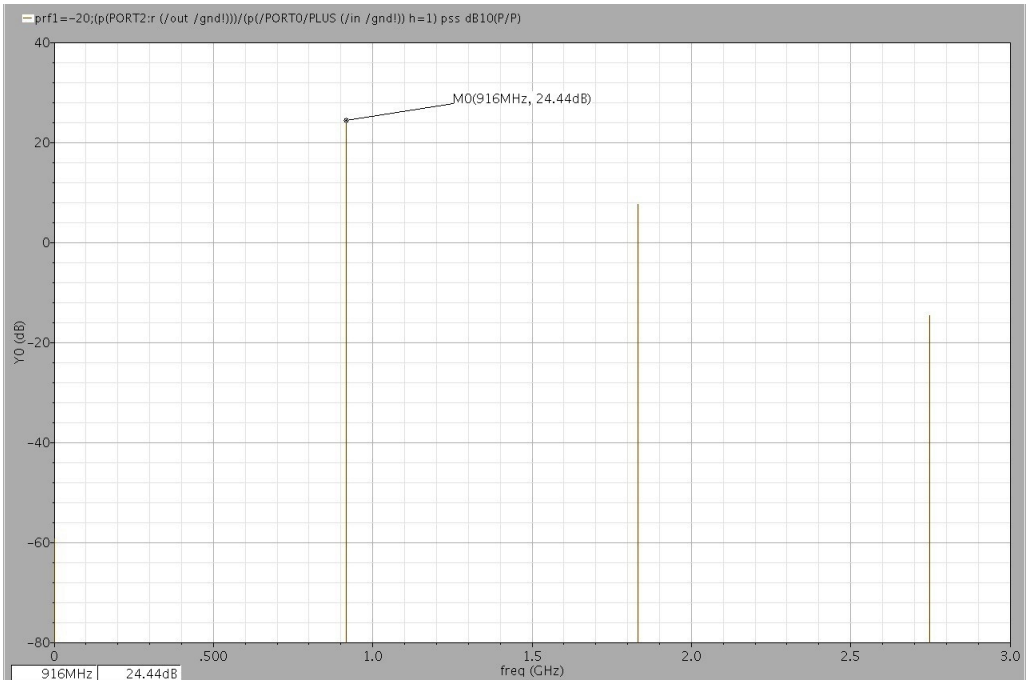

Figure 4.8 Power gain of the power amplifier

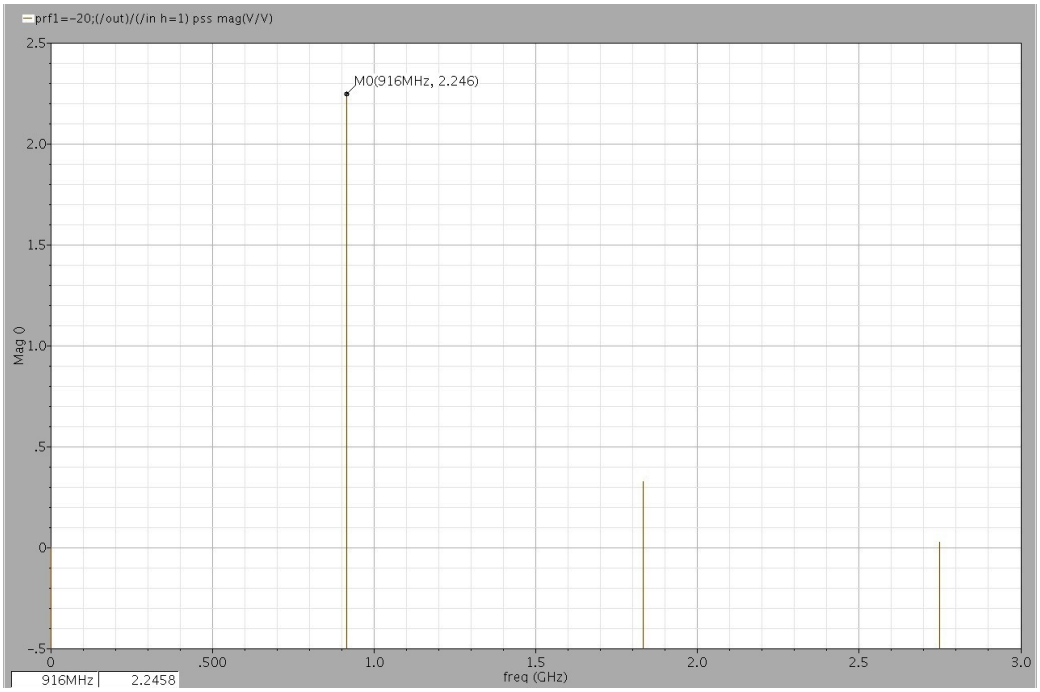

Figure 4.9 Voltage gain of the power amplifier

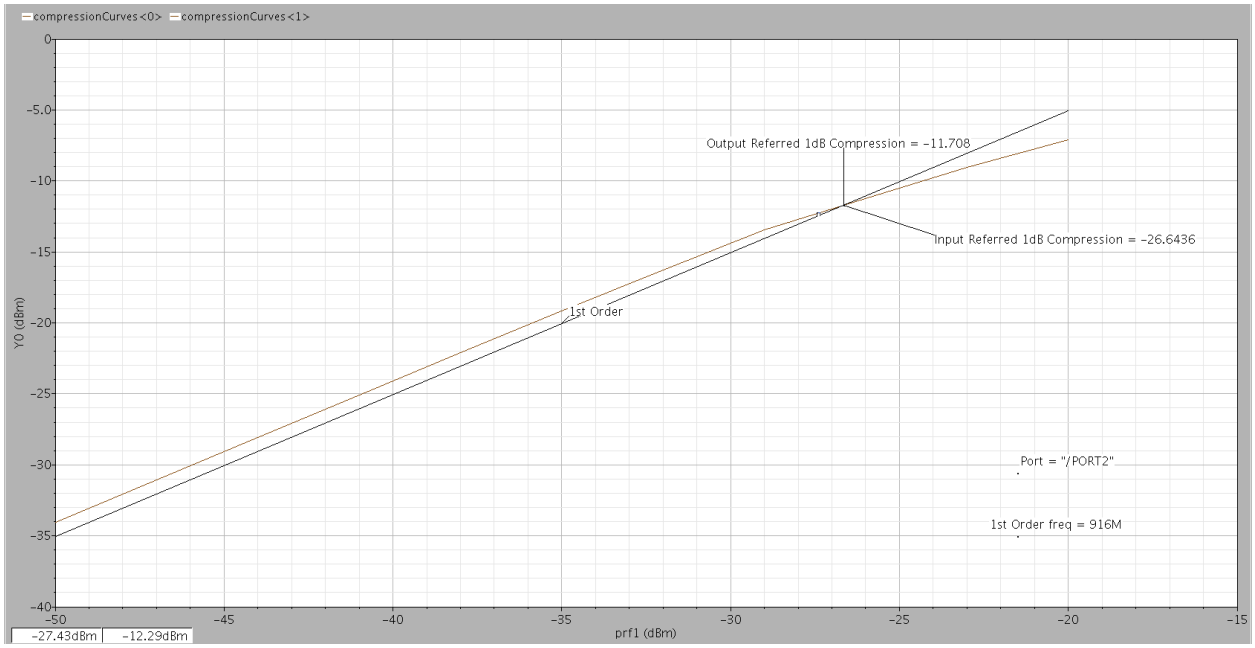

Figure 4.10 1-dB compression point of the power amplifier

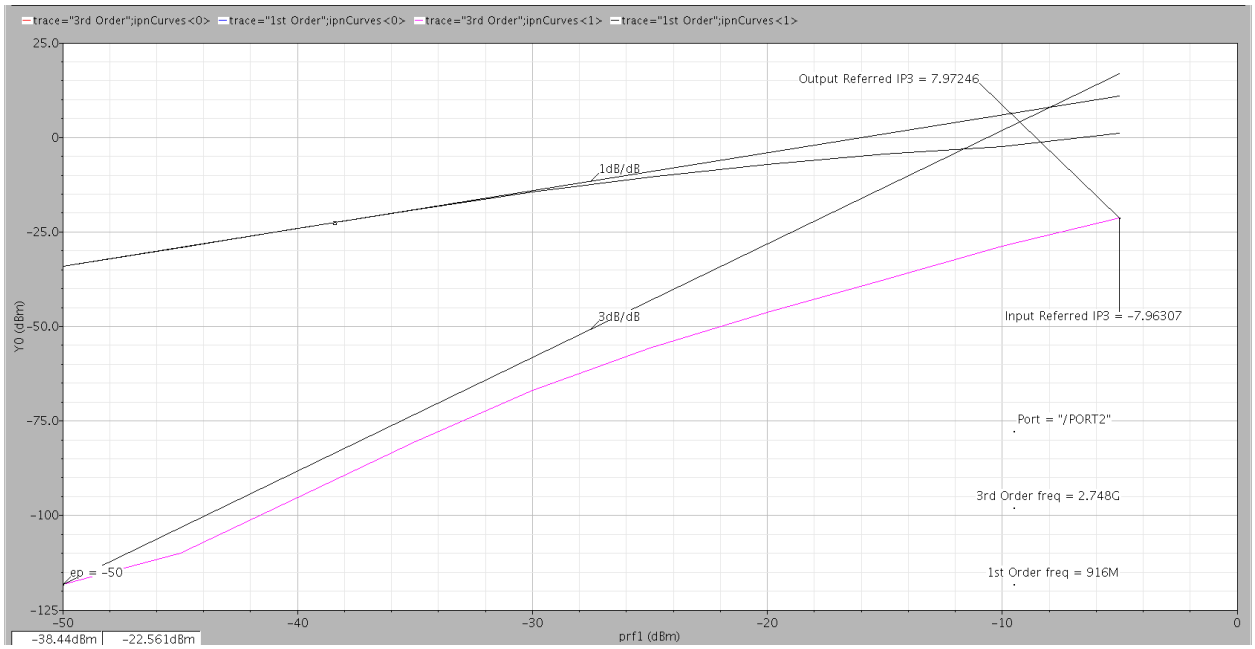

Figure 4.11 IP3 curves of power amplifier

4.3 Complete Circuit Simulation Results

The complete circuit containing the mixer followed by the power amplifier was simulated. The test bench is shown in Figure 4.12. A -20dBm sinusoidal signal of 916MHz was applied to a balun. The balanced differential output from the balun was connected to the RF inputs of the circuit. The digital BBIC data signal of 10 MHz square wave with amplitude varying between 0 and 1.2 V has been applied to the 'local-'input of the circuit. The 'local+' input of the circuit has been connected to a V_{DD} of 1.2V. A bias voltage of 0.7V for the mixer bias circuit has been applied to the V_{dc} input. The circuit's differential output was coupled to a balun.

The following simulations were performed and the results are shown below:

1. The transient analysis was performed on the circuit and the amplified ASK modulated signal is shown in Figure 4.13.

2. The power gain and voltage gain were simulated. A power gain of 19.67 dB was obtained for the output harmonic of 926 MHz and is shown in Figure 4.14. A voltage gain of 0.6364 V/V was obtained for the output harmonic of 926 MHz and is shown in Figure 4.15.

3. The input referred 1-dB compression point of -22dBm for the output harmonic of 926 MHz was observed as shown in Figure 4.16.The input referred IP3 value of -11dBm was obtained by performing a two tone analysis and is shown in Figure 4.17. The average power dissipation of 600mW was observed.

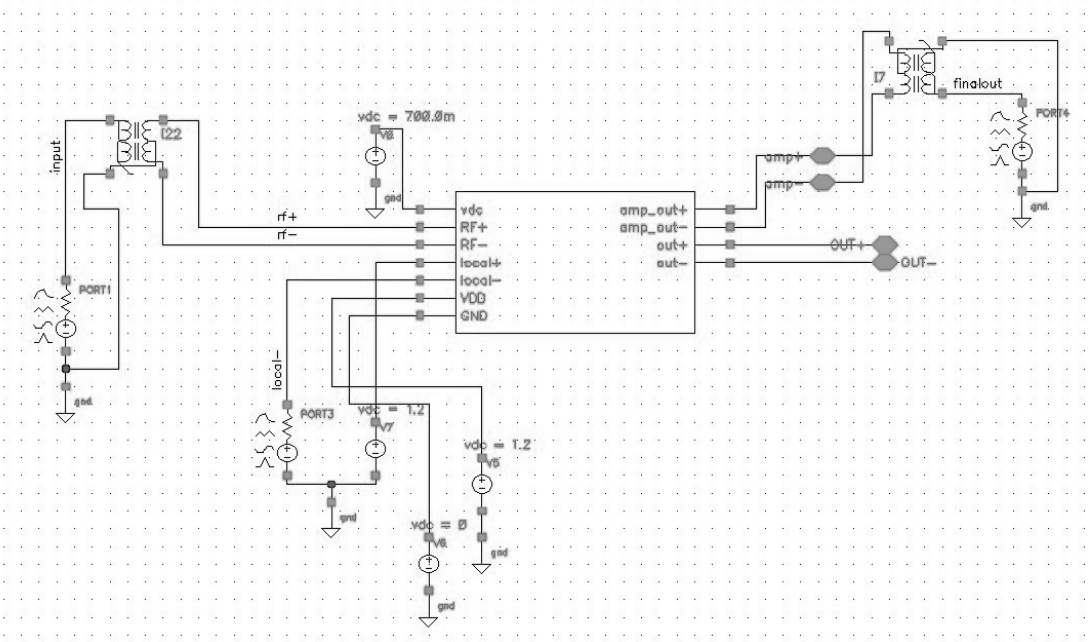

Figure 4.12 Test bench setup for the simulation of the complete circuit

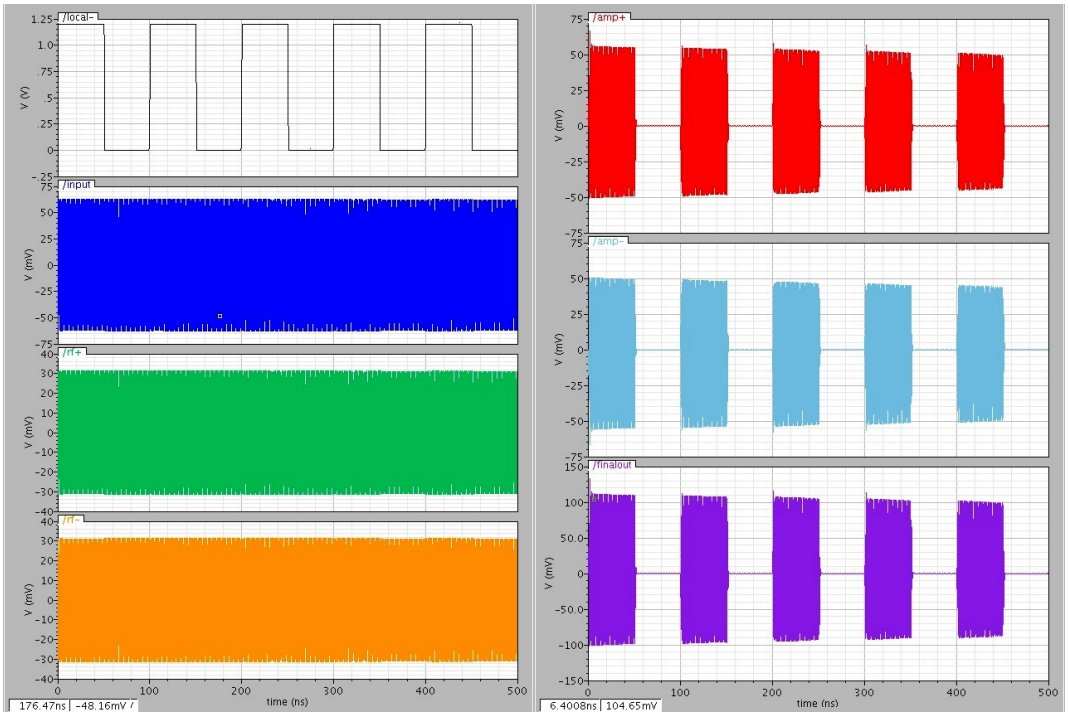

Figure 4.13 The amplified ASK modulated signal obtained by performing transient analysis

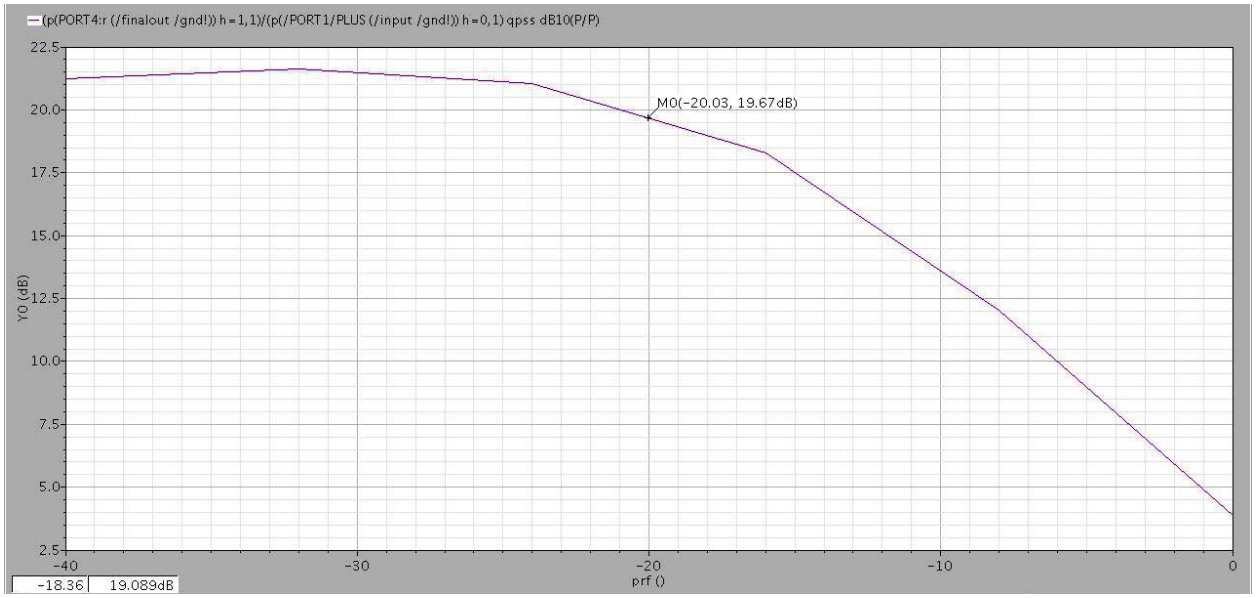

Figure 4.14 Power gain of the complete circuit

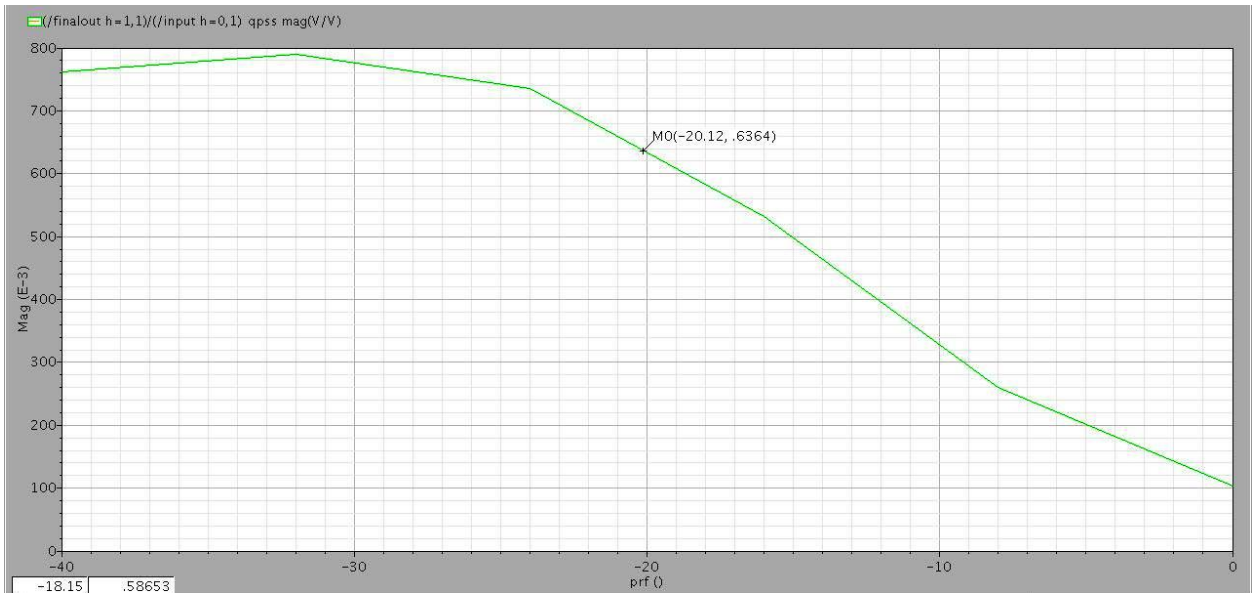

Figure 4.15 Voltage gain of the complete circuit

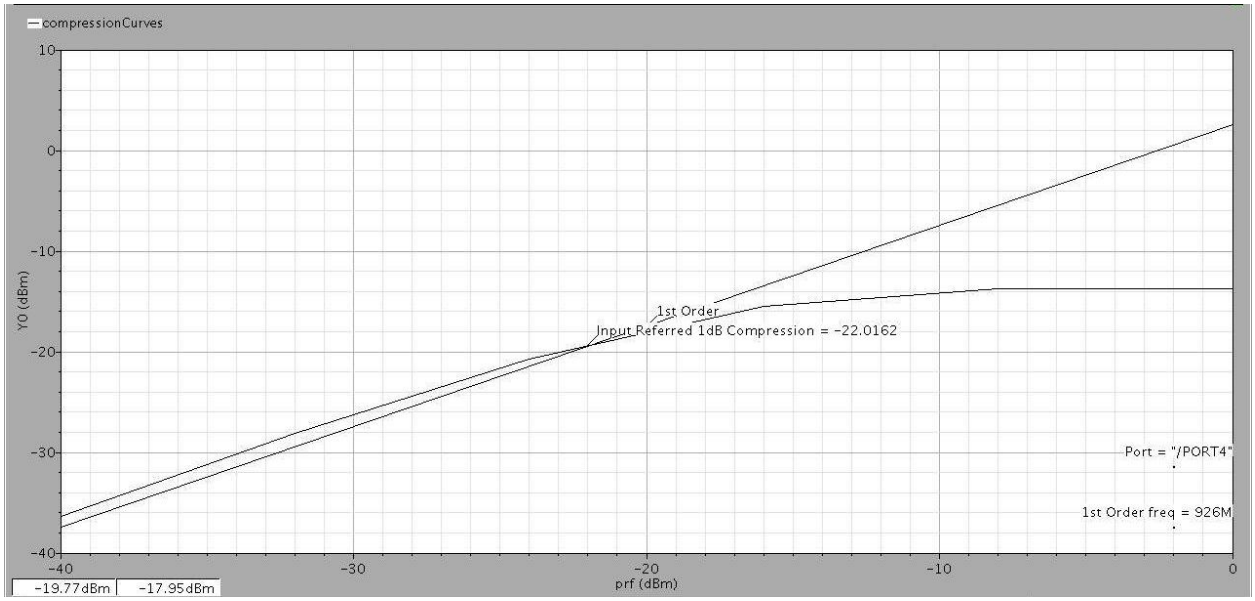

Figure 4.16 1-dB Compression point of the complete circuit

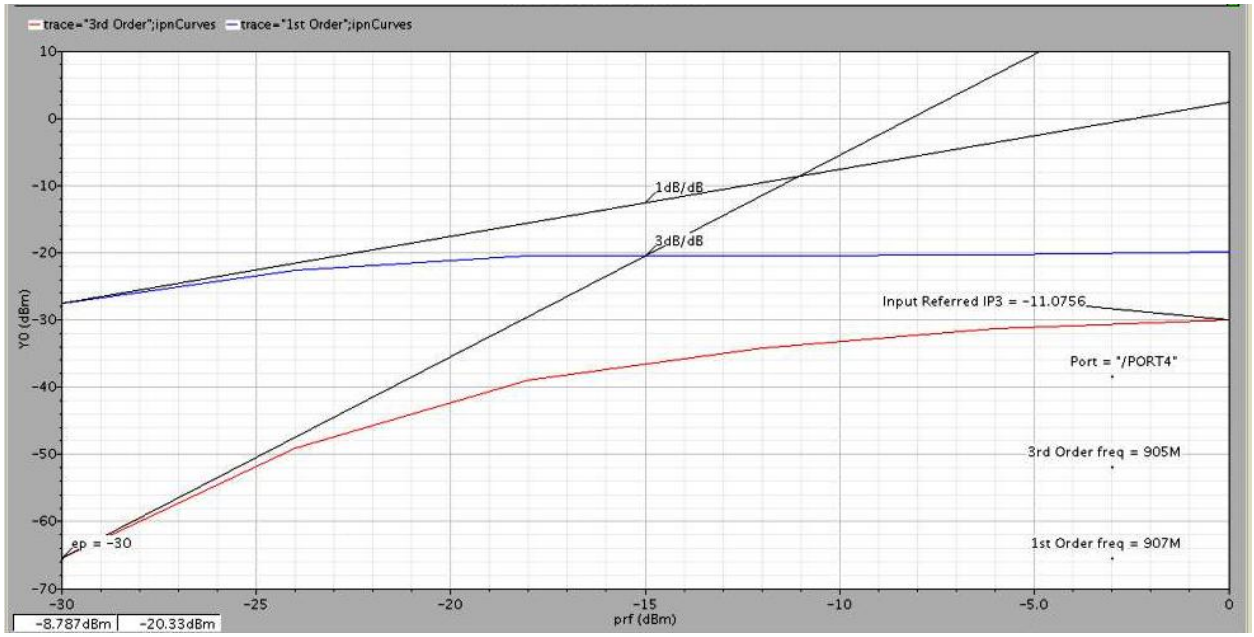

Figure 4.17 IP3 value of the complete circuit

4.4 Input Matching Network

The input matching network was designed and included on the test board. The quality of the input matching network was measured with the scattering parameter measurements. The L-type input matching network was used to match the circuit's input impedance to the source impedance of 50Ω. The load impedance of the circuit was almost equal to the 50Ω and hence an output matching network was not used. The input scattering parameter S_{11} was -6.76dB and the output scattering parameter S_{22} was -22dB at 916MHz. They are shown in Figure 4.18.

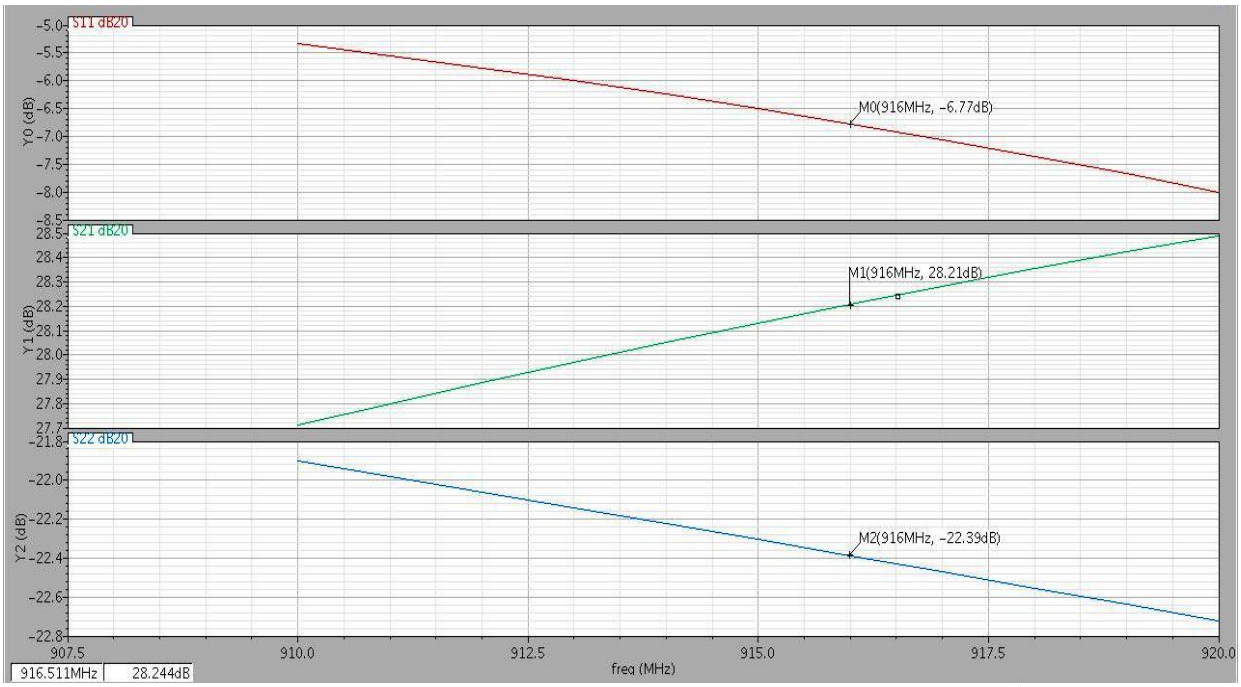

Figure 4.18 S-parameters of the input matching network

4.5 Layout of the Complete Circuit With I/O Pads

The total area of the circuit was found to be around 2.4 mm^2.

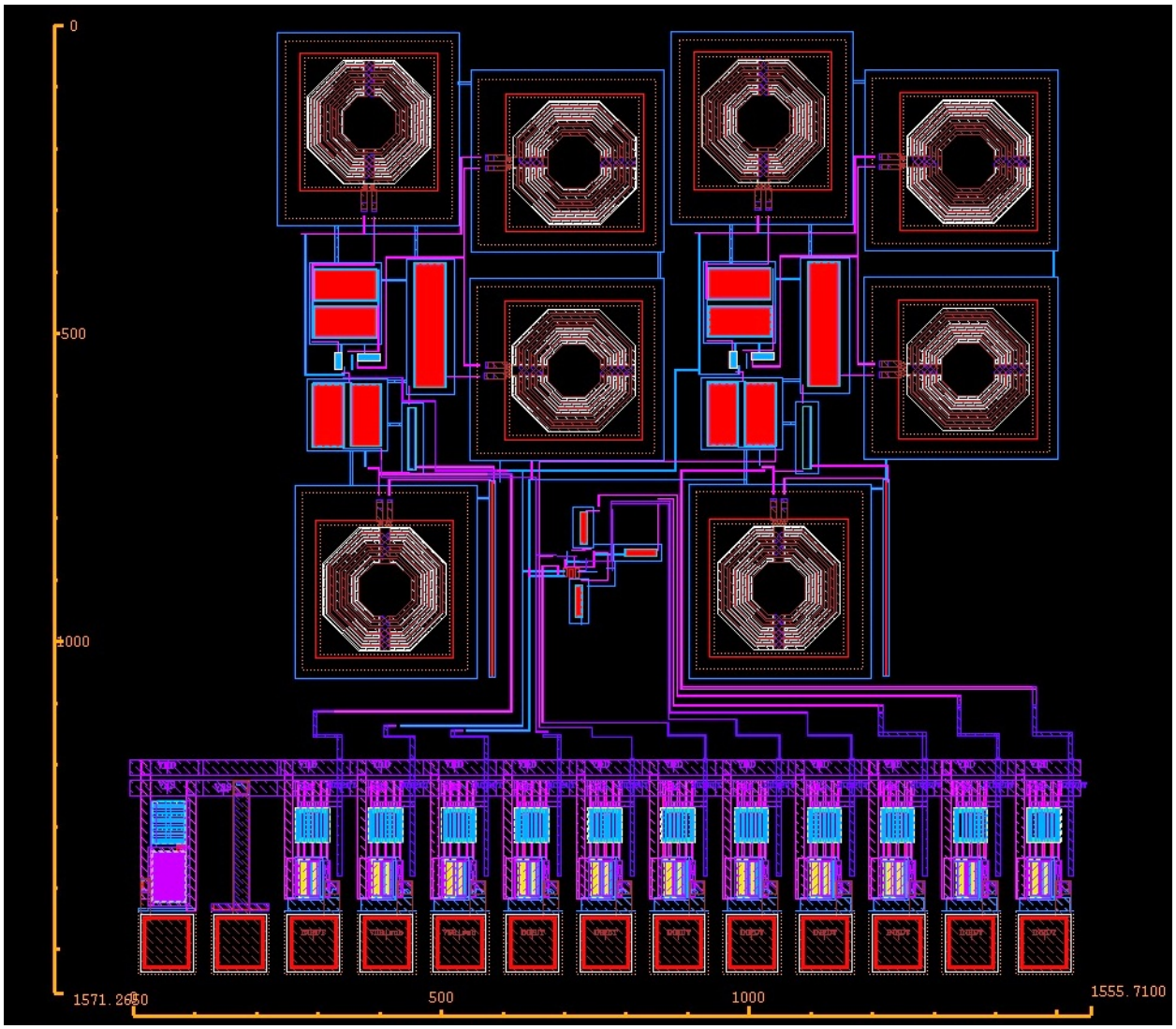

Figure 4.19 Layout of the complete circuit with the I/O pads

4.6 Post Fabrication Testing

4.6.1 Microphotograph of the Fabricated Chip

The microphotograph of the fabricated chip is shown in Figure 4.20.

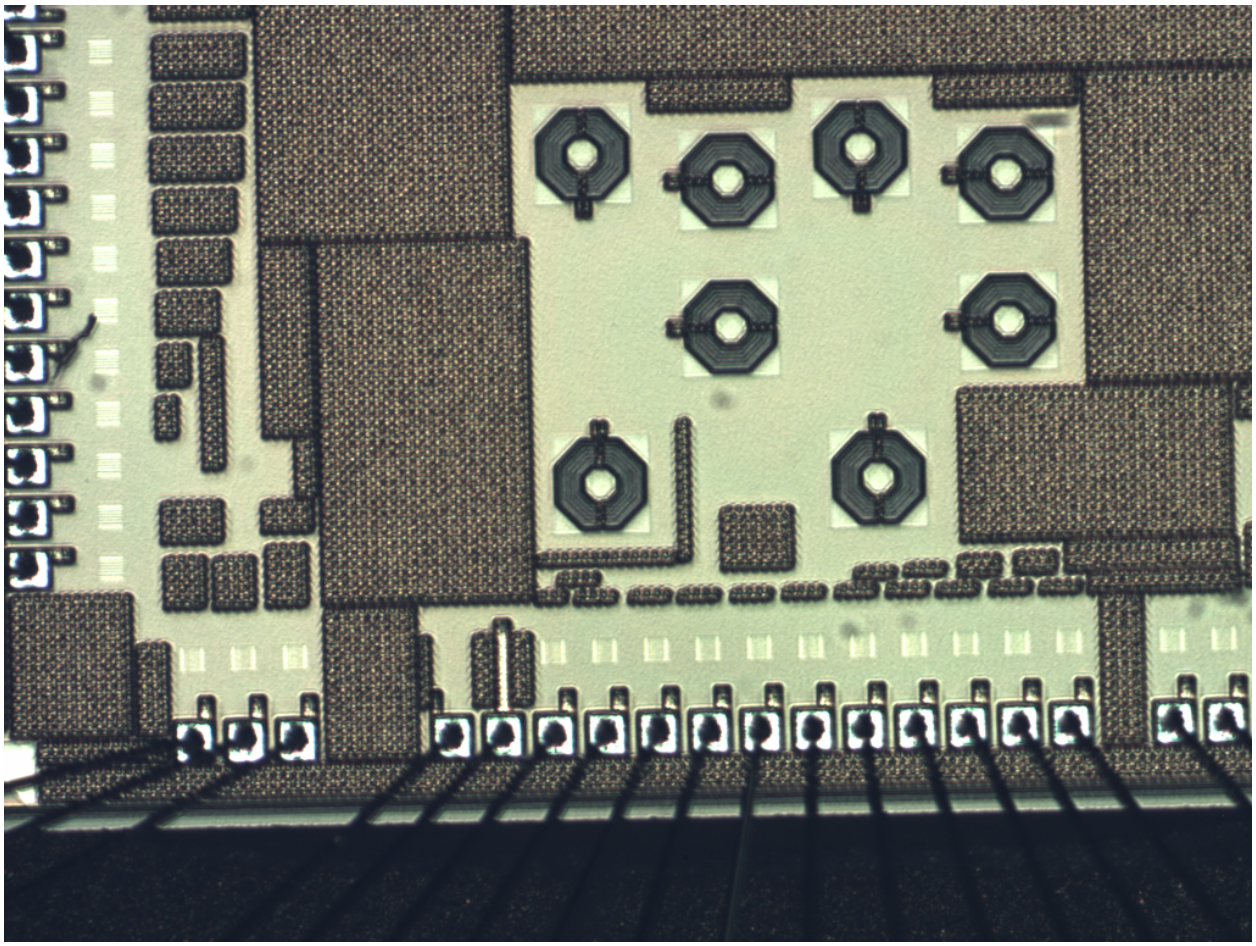

Figure 4.20 Microphotograph of the fabricated chip

4.6.2 Prototype Test Board

The prototype test board was designed to allow access to RF input/output, baseband digital input, mixer bias voltage and other power supply inputs. The PCB is constructed from FR4 material using a two-layer board. A surface mount balun was used to convert the single ended RF input to differential inputs and the differential outputs to single ended output. The RF inputs were conjugate matched to the mixer's differential inputs by a L-type matching network. The prototype test board is shown in Figure 4.21.

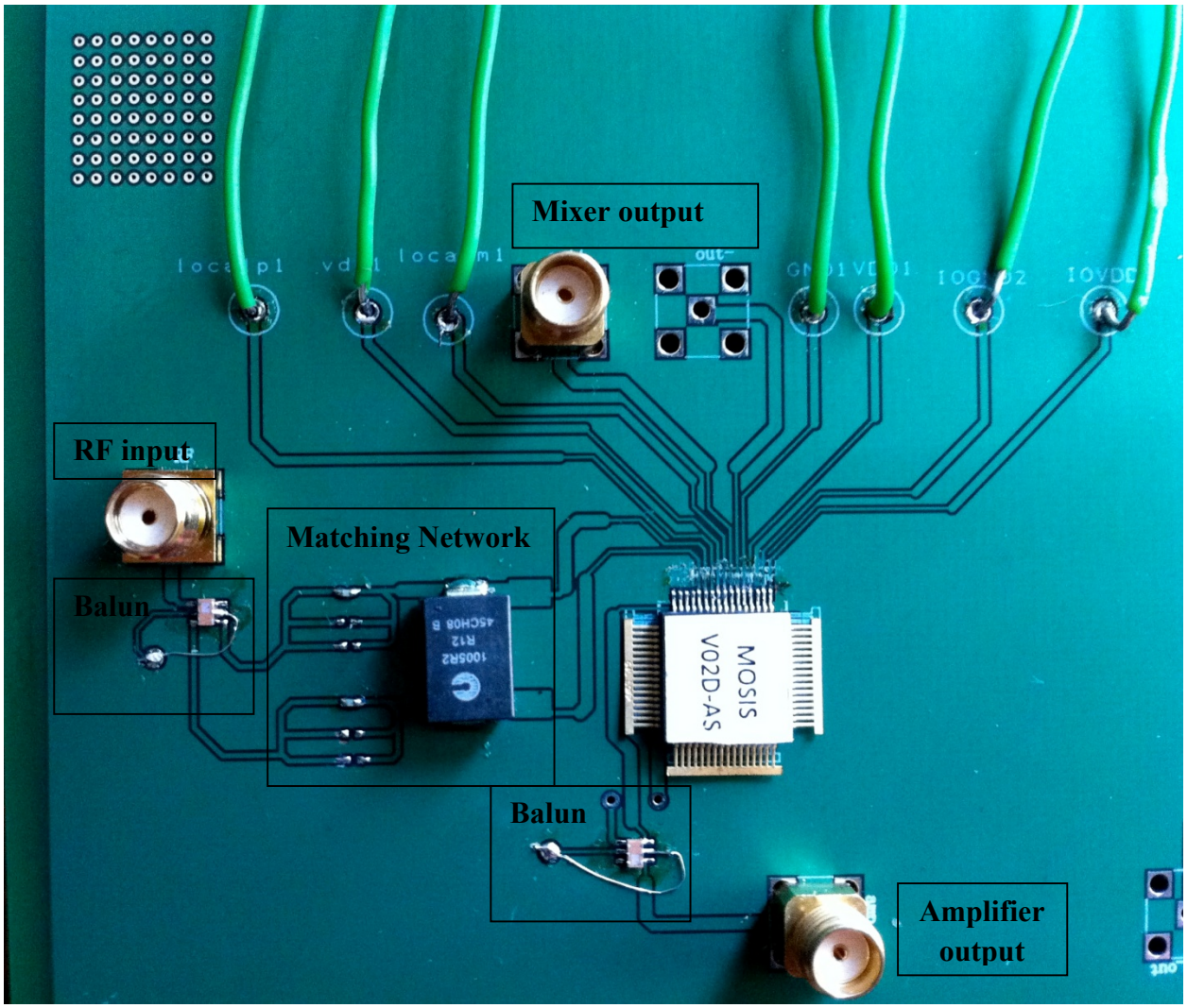

Figure 4.21 The prototype test printed circuit board

4.6.2 Test Setup

The complete test setup is shown in Figure 4.22. A RF generator was used to generate the -20 dBm 916MHz signal (Figure 4.23). A function generator was used to generate the 10MHz digital square wave signal with amplitude varying between 0 and 1.2 V (Figure 4.24). The output was seen on a spectrum analyzer and a digital oscilloscope. The other power supply connections are shown in Figure 4.24.

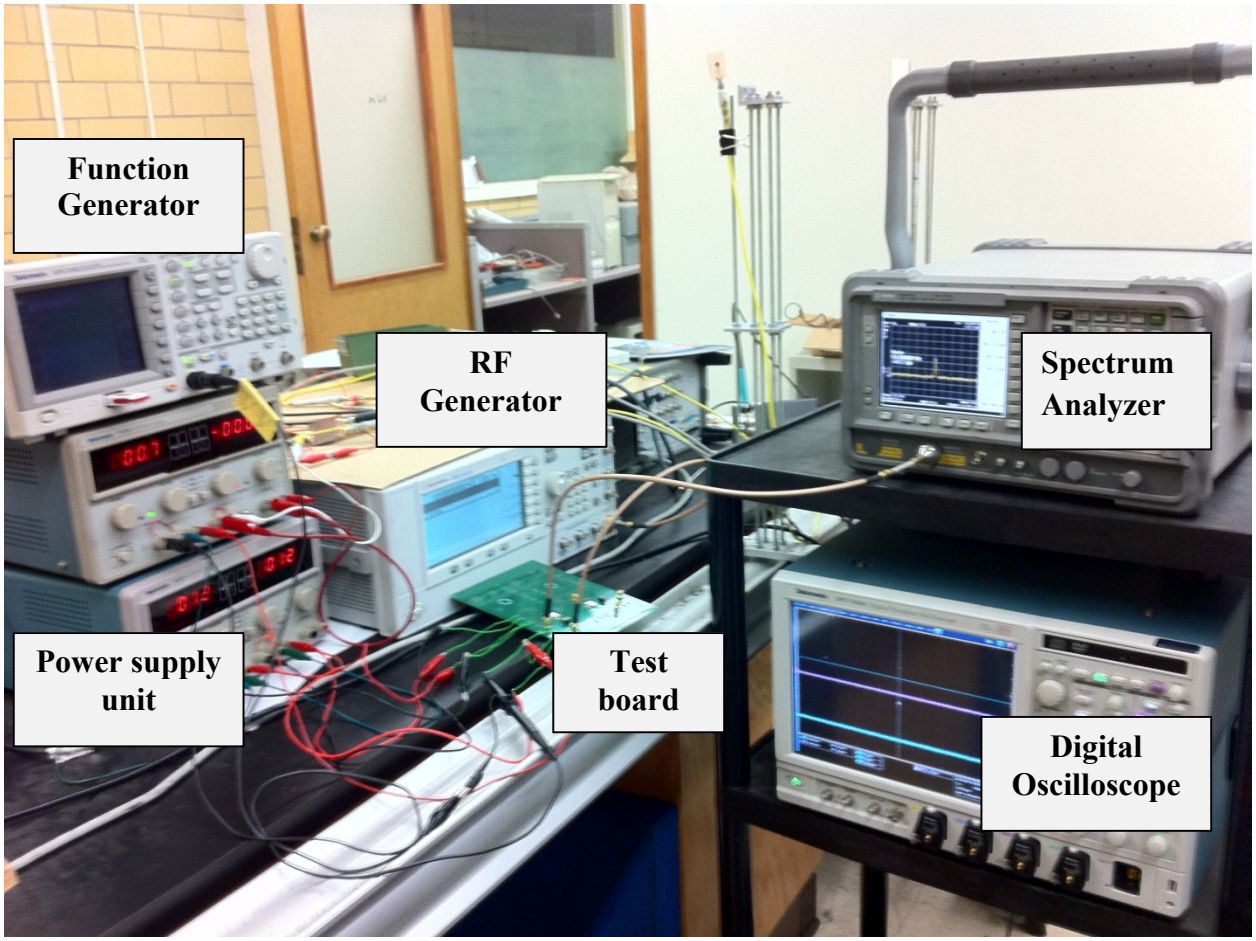

Figure 4.22 The complete test setup

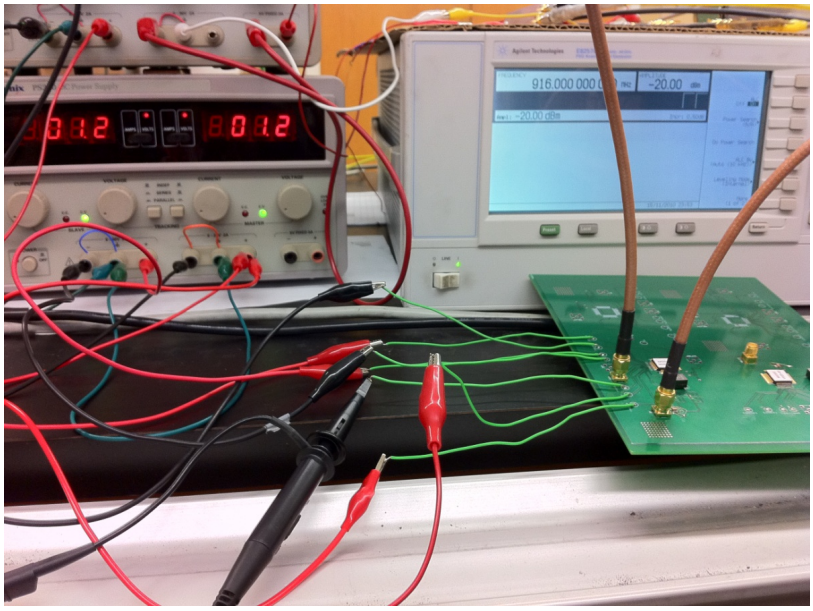

Figure 4.23 Test setup showing the input from the RF generator

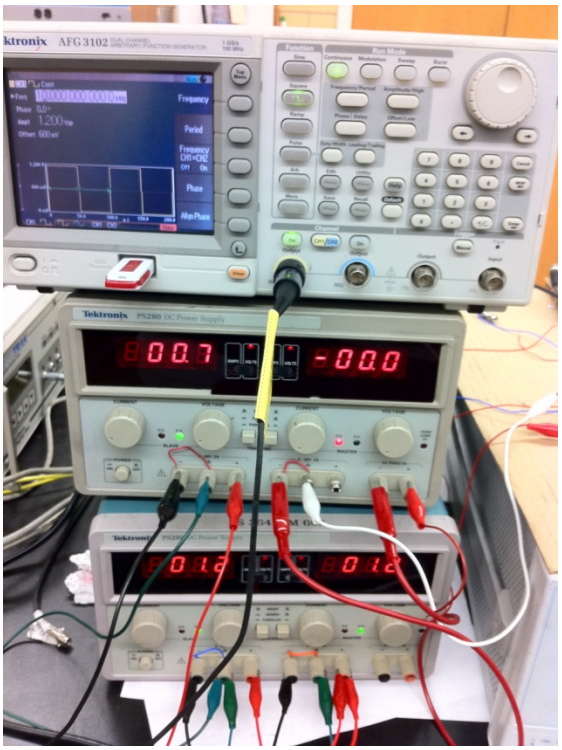

Figure 4.24 Test setup showing the inputs from the function generator and power supply units

4.6.3 Test Results and Analysis

The test results obtained from the above test setup are presented in this section. Figure 4.25 shows the power spectrum of the output. The output has also been viewed on a digital oscilloscope and is shown in Figure 4.26

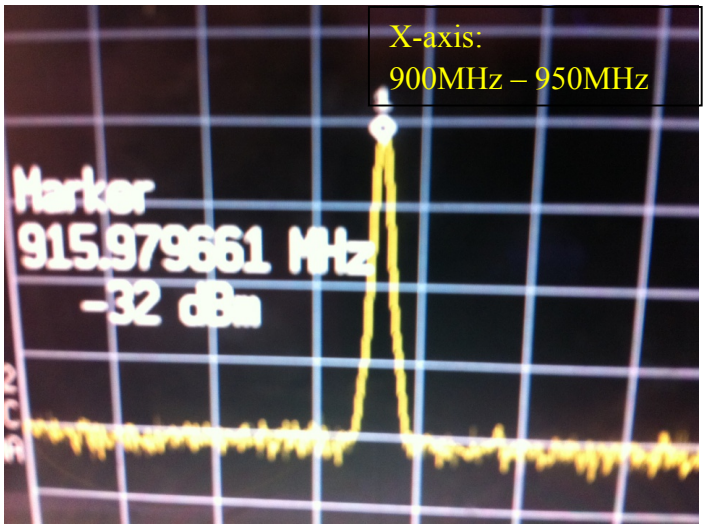

Figure 4.25 Output observed on a spectrum analyzer

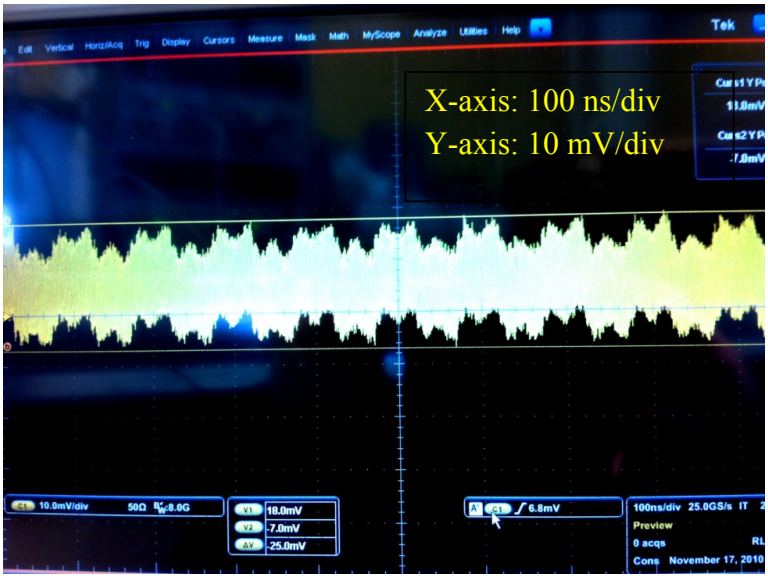

Figure 4.26 Output observed on a digital oscilloscope

Unfortunately, the output obtained was not as expected. It was seen from the spectrum analyzer that a noticeable power in the output was obtained only at 916 Mhz and not for the mixed products at 906 MHz and 926 MHz. However from the digital oscilloscope it was observed that mixing was taking place with a shift in the amplitude, but a significant change in the amplitude of the output was not observed. It can be seen that the amplitude of the output is not zero when digital "0" is being transmitted. By careful observation it was noticed that the carrier signal of 916 MHz is predominant throughout the output signal. Further debugging was done to find out the reason for the input carrier of 916 MHz being coupled to the output when digital "0" was being transmitted.

It was learnt during the debugging that the simulation results presented earlier did not include the I/O pads. The complete circuit was then simulated along with the I/O pads. The schematic including the I/O pads, balun and the matching network is shown below in Figure 4.27. It was observed form the simulation that the power supply head room changed due to the used of I/O pads. The I/O pads had a series resistance of around 290Ω which was responsible for the voltage drop. The current values at the V_{DD} pad and the GND pad were observed to be around 2 mA and 545 μA, respectively. This resulted in the V_{DD} and GND values to change to 590 mV and 155 mV respectively (Figure 4.28).With these V_{DD} and GND values to the core circuit the resultant voltage at the output node "out+" decreased and is shown in Figure 4.29.

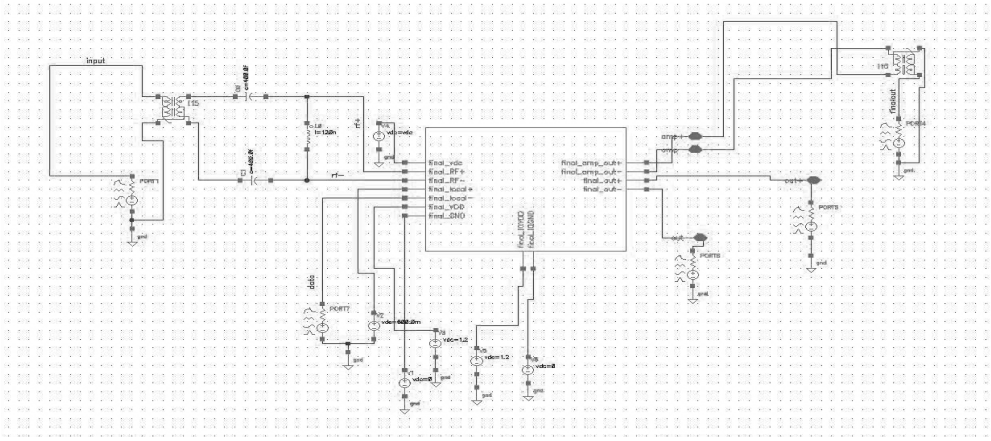

Figure 4.27 Schematic of the complete circuit with I/O pads, balun and matching network

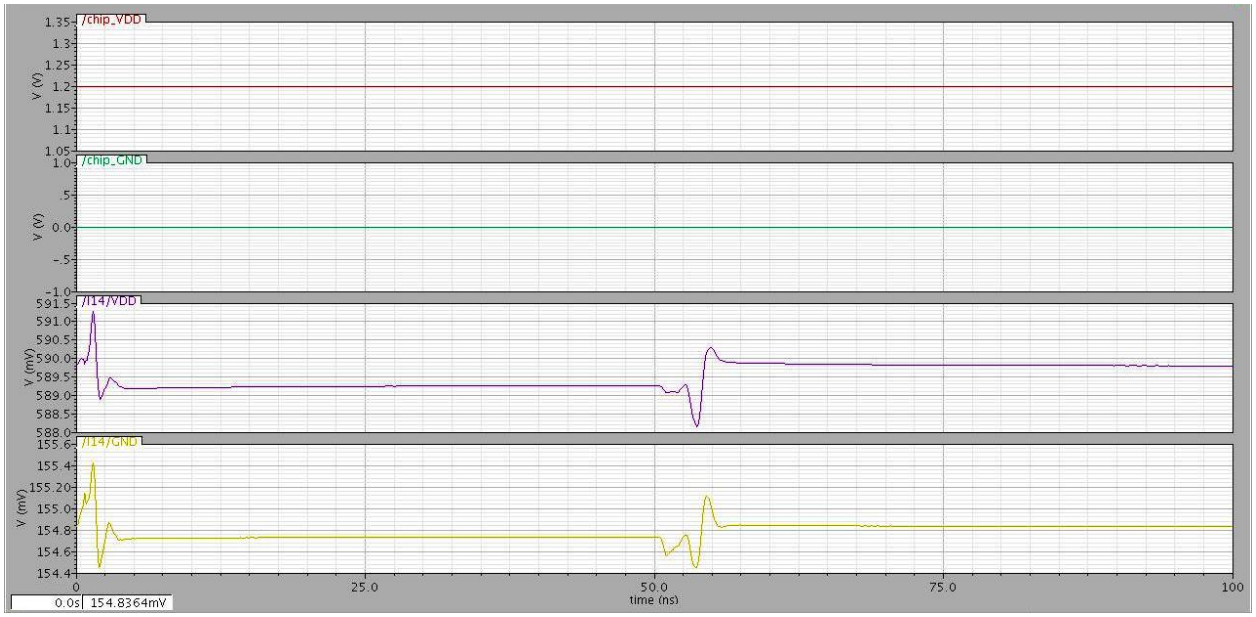

Figure 4.28 Graph showing the changed V_{DD} and GND values

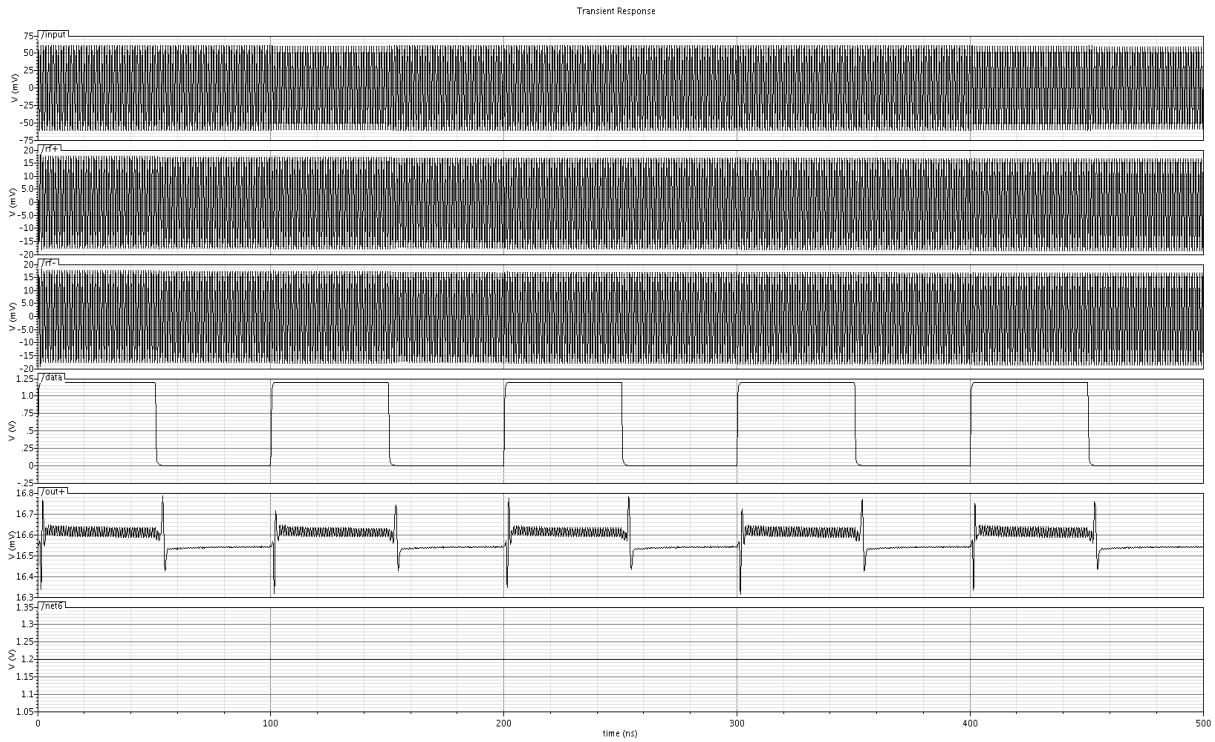

Figure 4.29 Transient response of the complete circuit with the I/O pads

Quasi-periodic steady state (QPSS) analysis was also performed to observe the power values of the mixed output products. The simulation result is shown in Figure 4.30. It was observed that the mixed products obtained were attenuated with the change in the V_{DD} and GND values. The mixer circuit simulation without the I/O pads where gain was obtained is also shown in Figure 4.31.

From both the transient and QPSS analyses it could be concluded that the simulation with the I/O pads results in the mixed output, but with attenuation. However, it was also observed that these simulation results do not have the RF input of 916 MHz being coupled to the output when digital "0" is being transmitted, as it was seen in the testing. Thus the debugging was continued to find out the reason for the coupling in the output.

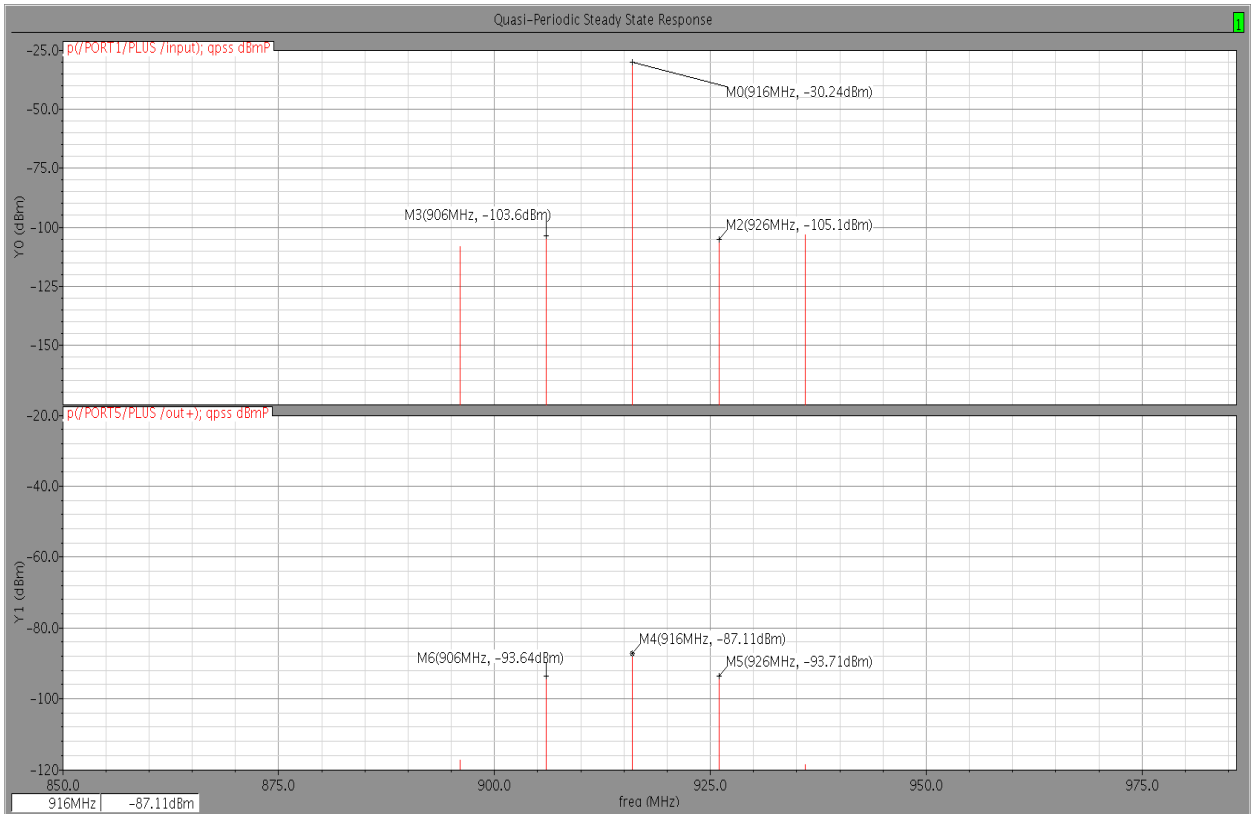

Figure 4.30 Quasi periodic steady state response of the complete circuit with I/O pads

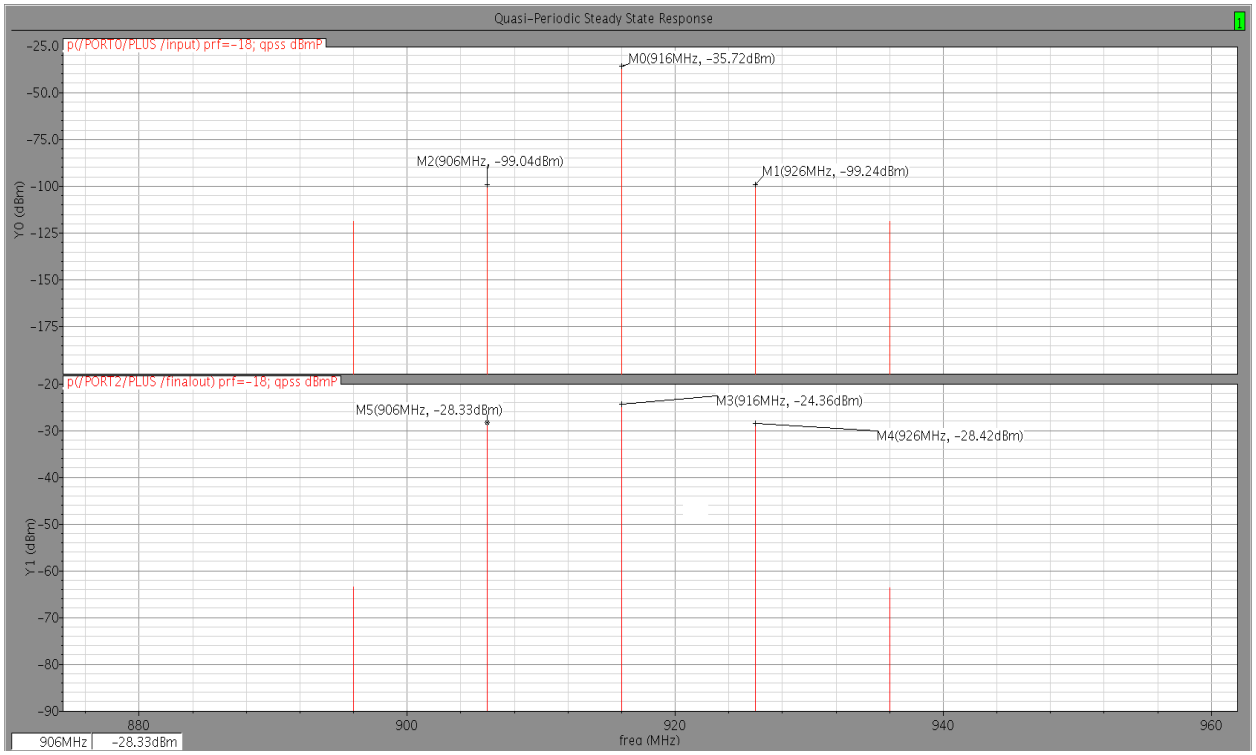

Figure 4.31 Quasi periodic steady state response of the mixer circuit without I/O pads

During testing it was noticed that the RF input of 916 MHz was coupling significantly to the output even when the other inputs and power supply were not given to the chip. To check on this the simulation was done only with the RF input and without supplying power and the other inputs. The simulation did not result in any significant coupling at the output node and is shown in Figure 4.32.

The testing was further continued by supplying only the RF input to the printed circuit board at different frequencies and the output was observed. The results are provided in the table 4.1 below. From these results it can be concluded that at high frequencies significant capacitive coupling of the RF input to the output is taking place even in the absence of power supply and other inputs.

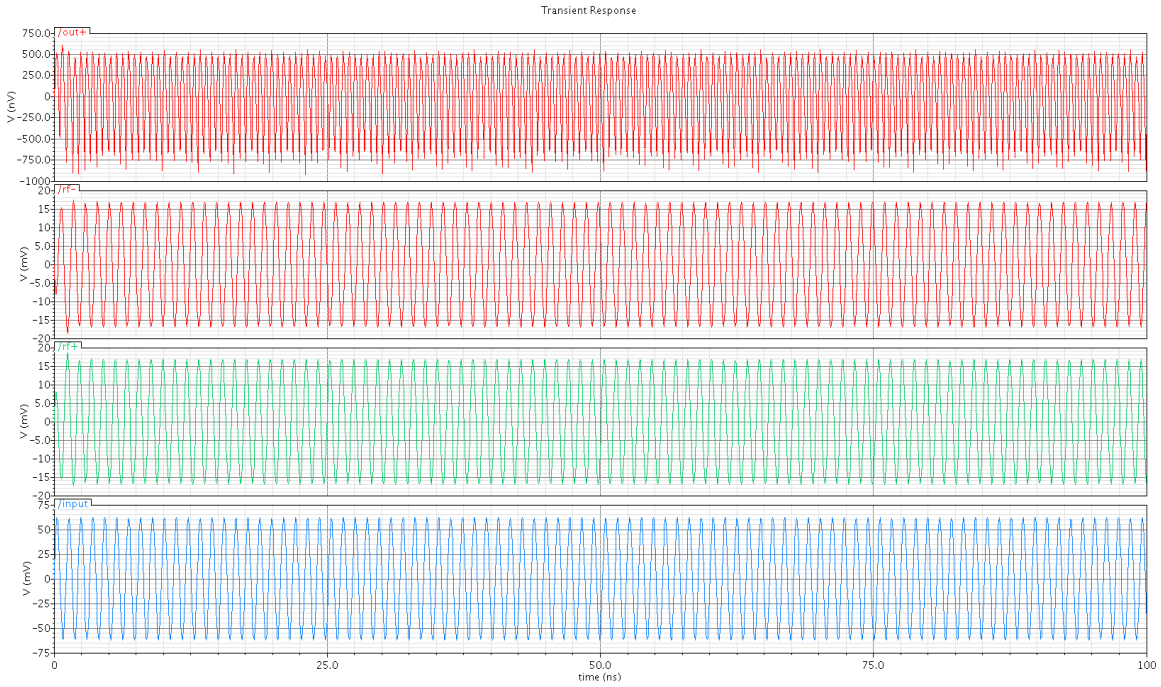

Figure 4.32 Simulation performed only with the RF input

Table 4.1: Printed circuit board tested at different frequencies

Frequency (MHz)	RF input (dBm)	Output at "out+" (dBm)
100	-38	-64
500	-24	-48
700	-18	-49
900	-19	-39
916	-21	-36
1000	-18	-40
2000	-14	-39
3000	-10	-44
5000	-7	-52
7000	-7	-43

The significant capacitive coupling of the RF input to the output node in the absence of other inputs and power supply should be a PCB design issue. On critical review of the PCB design it was learnt that all the connections made were correct but the top copper pour was left floating unlike the bottom copper pour which was grounded. This floating top copper is responsible for the capacitive coupling of the RF input to the output.

It can be observed from the Table 4.1 that at 916 MHz, an input of -20 dBm results in an output of -36 dBm through capacitive coupling. This coupling is observed to be more significant than the outputs obtained through the QPSS analysis in Figure 4.30. Hence the mixed output products are being surpassed by the direct RF capacitive coupling. Therefore the test results observed on the digital oscilloscope had RF carrier even when digital “0” was being transmitted though the mixing was taking place.

Chapter 5

Conclusion

5.1 Conclusion

The purpose of this thesis was to have a first on-chip transmitter for the BBIC. A low power double balanced Gilbert cell mixer and a Class A power amplifier have been designed for the BBIC transmitter. Reasonable gain and linearity were achieved by the Gilbert cell mixer. Having the transconductor transistors of the Gilbert cell mixer operate in the subthreshold region the power consumption was also reduced. However the Class A power amplifier performance in terms of linearity was poor. The simulation results were encouraging.

5.2 Future Work

Though the simulation results were encouraging, it was learnt from the testing that I/O pads used in the layout resulted in an attenuated output. Moreover the floating top copper pour of the PCB design resulted in capacitive coupling of the RF input to the output. Therefore it is required to redesign the PCB with the top copper pour grounded and have the layout of the chip with I/O pads that do not use a series resistance to obtain the expected results.

The performance of the Class A power amplifier can be improved in terms of linearity by using linearization techniques. Also the Class A power amplifier has a poor performance in terms of efficiency. So a more efficient power amplifier can also be considered for the transmitter.

A Phase locked loop (PLL) needs to be developed for the transmitter system. It is required to generate the 916 MHz carrier signal. If the PLL is developed then we can have the entire transmitter for the BBIC on chip. Finally an interface to the antenna needs to be developed.

References

[Bolton] Eric Keith Bolton, A CMOS microluminometer for use in a bioluminescent bioreporter integrated circuit, Thesis (M.S.), University of Tennessee, Knoxville, 2001.

[Islam] Syed K. Islam et al., IEEE Transactions on circuits and systems, Vol. 54, No. 1, January (2007).

[Lathi] B P Lathi, Communication Systems, New York, Wiley, 1968.

[Razavi] Behzad Razavi, RF Microelectronics, Prentice Hall, 1998.

[Couch] Leon W. Couch, Digital and analog communication systems, Macmillan Publishing Company, 1990.

[Arya] Behzad Arya, Wireless LAN Radios – System definition to transistor design, Wiley, 2008.

[Zhang] Mo Zhang, A low power CMOS microluminometer and transmitter for bioluminescent bioreporter integrated circuit (BBIC), Thesis (M.S.), University of Tennessee, Knoxville, 2003.

[Carr] Joseph J Carr, RF components and circuits, Oxford :Newnes, 2002.

[Jeremy] Everard Jeremy, Fundamentals of RF circuit design : with low noise oscillators, John Wiley, c2001.

[Ding] YongWang Ding, High-linearity CMOS RF front-end circuits, Springer, 2005.

[Arnott] James C Arnott, A PLL frequency synthesizer and Gilbert cell multiplier for a 916 MHz ISM band transmitter realized in 0.5 [mu] m [i.e. micrometer] CMOS technology, Thesis (M.S.)--University of Tennessee, Knoxville, 1999.

[Terry] Stephen Christopher Terry, Development of a high-efficiency, low-power RF power amplifier for use in a high-temperature environment, Thesis (M.S.)--University of Tennessee, Knoxville, 2002.

[Lee] Hanil Lee, Saeed Mohammadi, " A 500μW 2.4 GHz CMOS subthreshold Mixer for Ultra Low Power Applications", 2007 IEEE Radio Frequency Integrated Circuits Symposium.

[Sullivan] P. J. Sullivan, B.A.Xavier, and W.H.Ku, “Low Voltage Performance of a Microwave CMOS Gilbert Cell Mixer”, IEEE J. of Solid-State Circuits, Vol. 32, No. 7, July 1997.

[Rudell] Jacques C.Rudell, Jia-Jiunn Ou, Thomas Byunghak Cho, Geroge Chien, Francesco Brianti, Jeffrey A. Weldon, and Paul R. Gray, “A 1.9-GHz Wide-Band IF Double Conversion CMOS Receiver for Cordless Telephone Applications”, IEEE J. Solid-State Circuits, Vol. 32, No. 12, December 1997.

Vita

Supriya Kilambi was born on March 12, 1986, in Hyderabad, Andhra Pradesh, India. She completed her high school from Sri Aurobindo International School and her under graduation from Osmania University, Hyderabad in Electronics and Communication Engineering. She joined the University of Tennessee, Knoxville in the Electrical Engineering and Computer Science Department in Spring 2008. In the same semester she joined as Graduate Research assistant in Innovating Computing Lab at UTK where she worked on VHDL programming. In the next semester she joined the Analog VLSI and Devices Laboratory at UTK and worked as Graduate Research assistant until May 2009.As a graduate research assistant she worked with circuit design and layout using Cadence, printed circuit board design and labview programming. Currently she is working as a graduate assistant at Innovative Technology Consulting at UTK where she is responsible for maintaining a training lab of 15 laptops. She will be graduating in Dec 2010. Her research mainly focuses on analog and mixed signal IC design.